Other reference :
ESTEC/Contract N°4000102571/10/NL/AF
Type :
Description :
Radiation Characterization of LAPLACE/TANDEM RH Optocouplers, Sensors and Detectors
Title of document :
HAS2 Proton DDD Report

	Names	Dates
Prepared by	VAN AKEN Dirk (ON Semiconductor) HERVE Dominique (Sodern) BEAUMEL Matthieu (Sodern)	23/11/2012
Checked by	-	-
Approved by	-	-
Customer approval	-	-

CHANGE RECORD	
Revision	Description of change
A	First issue

TABLE OF CONTENTS

1.SCOPE AND APPLICABILITY

1.1.Scope

This test report presents the result of the proton DDD irradiation of the HAS2 CMOS image sensor performed in the frame of ESTEC contract N° 4000102 571/10/NL/AF “Radiation Characterization of Laplace/Tandem RH optocouplers, sensors and detectors”.

The proton irradiations were performed at PSI in February 2012. The annealing steps at room temperature and elevated temperatures were performed at ON Semiconductor in October 2012.The reason for this delay was the activation of the parts which was only below an acceptable level after 8 months of room temperature annealing.

1.2.Purpose

The effect of proton DDD radiation and the annealing thereof is studied on the HAS2 in the ON and OFF state in all different possibilities such as ON during radiation and OFF during annealing and other possible combinations.

2.REFERENCES

2.1.Applicable documents

[AD 1] ITT 6429 HAS Irradiation Test Plan, PR__00004584, D

2.2.Reference documents

3.ABBREVIATIONS

AD	Applicable Document
APS	Active Pixel Sensor
CDS	Correlated Double Sampling
CMOS	Complementary Metal-Oxide Semiconductor
DC	DateCode
DDD	Displacement Damage Dose
DR	Destructive Readout
DS	Double Sampling
DSNU	Dark Signal Non Uniformity
ECSS	European Cooperation for Space Standardization
EOL	End Of Life
ESA	European Space Agency
FPN	Fixed Pattern Noise
HAS2	High Accuracy STR 2
LET	Linear Energy Transfer
LSB	Least Significant Bit
N/A	Not Applicable
NDR	Non-Destructive Readout
PCB	Printed Circuit Board
RD	Reference Document
SEE	Single Event Effect
SET	Single Event Transient
SEU	Single Event Upset
SEFI	Single Event Failure interrupt
TID	Total Ionizing Dose

4.DEVICE INFORMATION

4.1.HAS2 presentation

The Accuracy STR 2 sensor (HAS2) is a 1024 x 1024 pixel rolling shutter Active Pixel Sensor (APS), featuring a programmable (gain and offset) output amplifier (PGA) and an internal 12 bits ADC.

The CMOS image was sensor designed and manufactured by ON Semiconductor[1] under ESA contract 17235/03/NL/FM for star tracker applications.

The block diagram of HAS2 is presented in Figure 4-1.

Pixel design is based on a photodiode coupled with a three transistor readout circuit. The HAS2 is the descendant from a lineage radiation-hardened by design sensors from ON Semiconductor: the photodiodes includes a doped surface protection layer to prevent the depleted area from reaching the field oxide interface, while the CMOS readout circuitry is designed using enclosed geometry transistor layouts.

The wafers are produced by Plessey Semiconductors[2] on the standard XC035P311 CMOS process (0.35 µm).

In order to reduce the variation in signal offset from pixel to pixel (known as Fixed Pattern Noise, or FPN) typically seen on APS, the HAS2 implements two different noise reduction techniques: Double Sampling (DS) also called Destructive Readout (DR) and Correlated Double Sampling (CDS) also called Non Destructive Readout (NDR). In DR mode, the pixel is reset at the end of the signal integration time in order to sample the pixel reference level. The reference level is subtracted from the signal level in order to cancel the pixel offset. This internal analog operation is performed before digitization. In NDR mode, two images are sampled and digitized: a reference image at the beginning of the integration time, and a signal image at its end. Offset correction must be performed off-chip by subtracting these two images.

A temperature sensor is also integrated on chip, which can be addressed through an internal multiplexer. This MUX can also address analogue inputs to be digitized by the internal ADC.

[1] Formerly Cypress BVBA and Fillfactory.
[2] Formerly X-FAB.

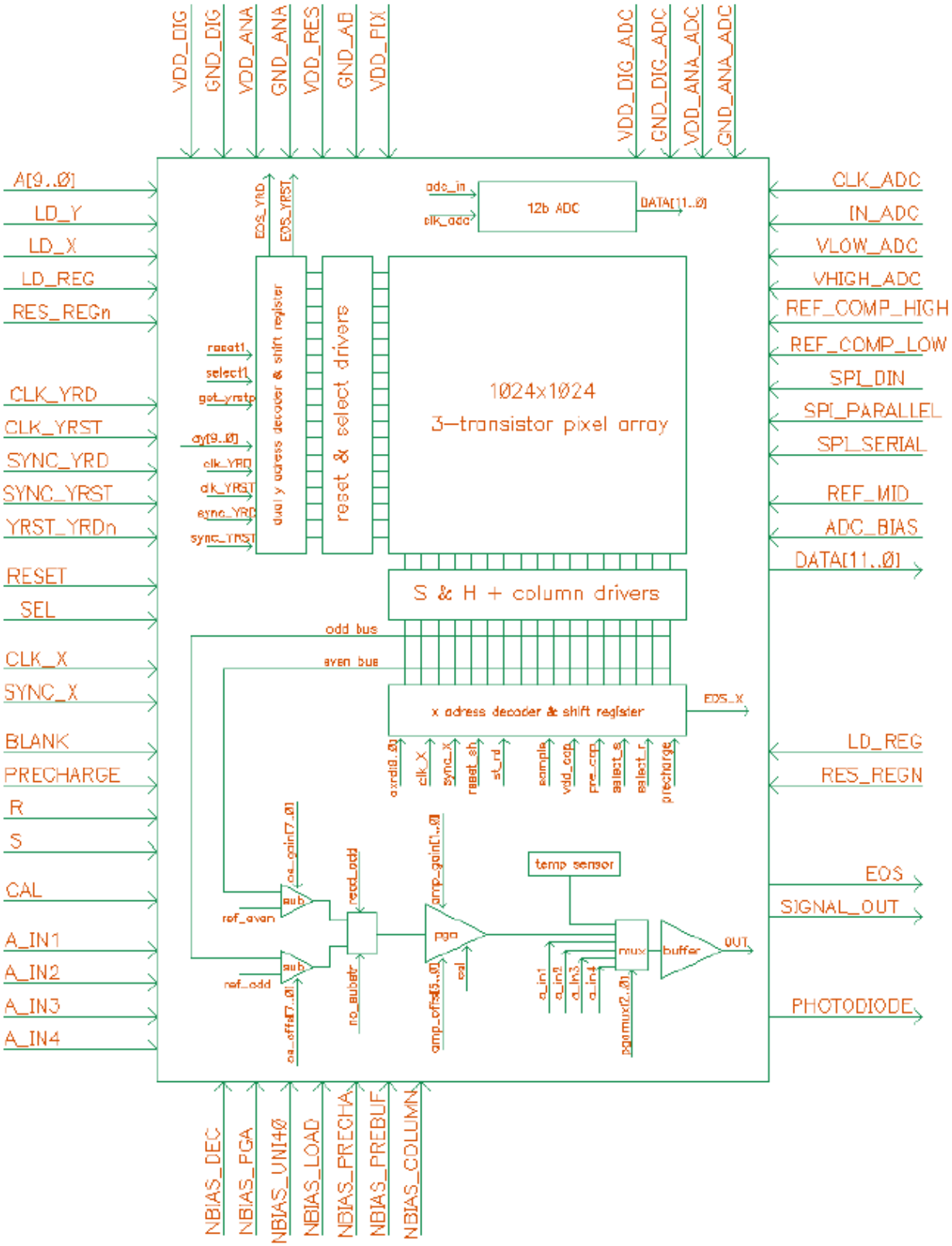

Figure 4-1 : HAS2 block diagram

Samples identification
Part type: HAS2
Manufacturer: ON Semiconductor
Package: JLCC84
Tested Samples:

164	Reference sample used during HAS ESCC evaluation campaign
674	Sample from wafer lot P29506.1
726	Sample from wafer lot P29506.1
719	Sample from wafer lot P29506.1
727	Sample from wafer lot P29506.1
708	Sample from wafer lot P29506.1
681	Sample from wafer lot P29506.1
671	Sample from wafer lot P29506.1
711	Sample from wafer lot P29506.1
675	Sample from wafer lot P29506.1
677	Sample from wafer lot P29506.1
710	Sample from wafer lot P29506.1
670	Sample from wafer lot P29506.1

Samples from wafer lot P29506.1:
Backside marking: NOIH2SM1000A HHC (Engineering Models)
Date code: 110414 (April 14, 2011)

All samples have been subjected to an operational burn in step at +125 degC during 168h.

5.IRRADIATION FACILITY

Irradiation have been performed at Paul Scherrer Institute (PSI – Switzerland), on the Proton Irradiation Facility (PIF) High Energy site. The PIF experimental set-up consists of the local PIF energy degrader, beam collimating and monitoring devices (Figure 5-1 and Figure 5-2).

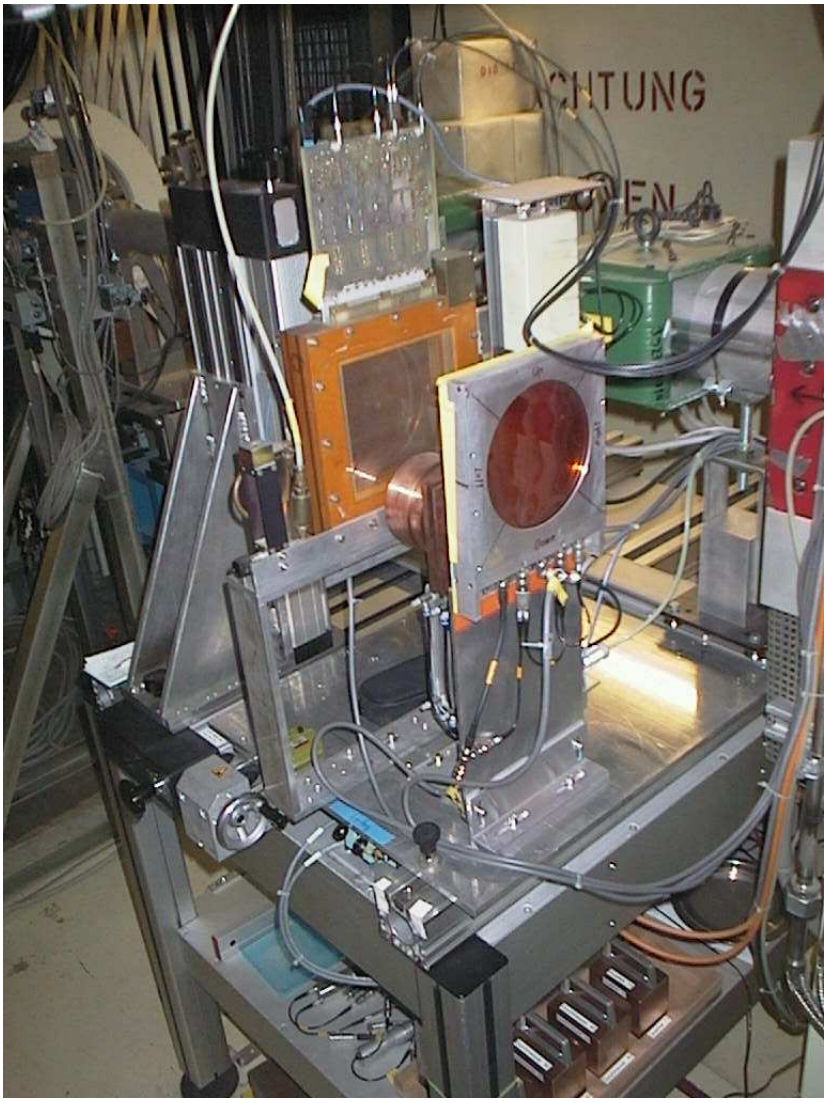

Figure 5-1 : PIF-PROSCAN downstream view with ionization chamber, energy degrader and wire chamber

Maximum beam intensity in the PIF area is around 2 nA for energies above 200 MeV, and 5 nA for energies from 100 MeV to 200 MeV. Delivered from PROSCAN accelerator used for cancer treatment, PIF exposures are mostly conducted during weekends and nightshifts. Irradiations are carried out in air. The maximum energy is 230 MeV. Beam diameter is 60 mm. Dosimetry is performed using the monitor detectors with an accuracy of the flux/dose determination of 5%. A laser pattern calibrated on the beam axis is used to place the DUT in the middle of the beam.

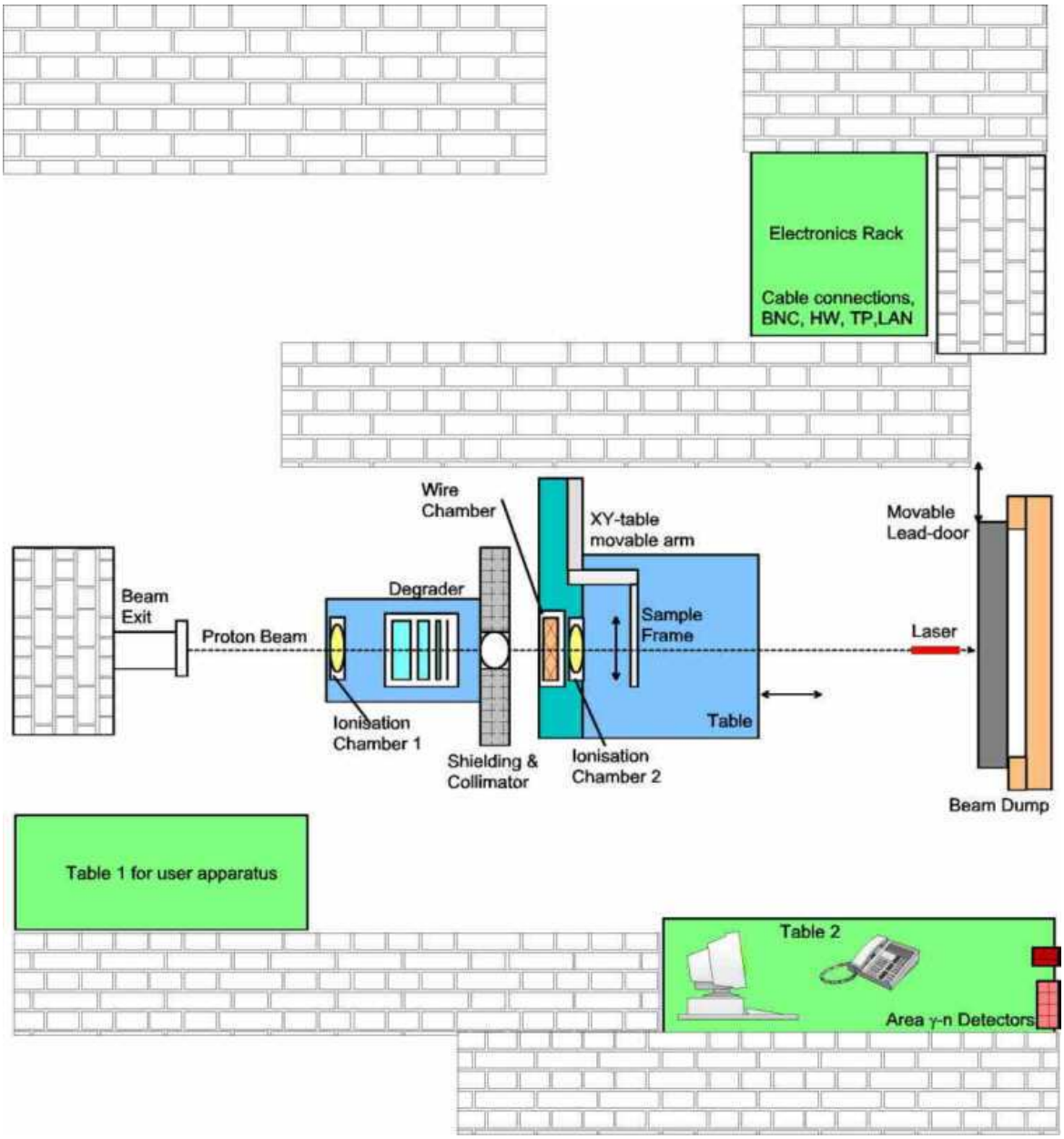

Figure 5-2 : PIF-PROSCAN experimental set-up layout

A proton flux of +/- 2.0E+08 protons/cm²/s was applied. The following energies were selected:

Energy [MeV]	*Range [mm Si]*	*LET [e-/µm]*
100	4.18E+01	3.78E+02
175	1.11E+02	2.56E+02
230	1.76E+02	2.15E+02

Table 5-1 : proton range and stopping power in silicon versus energy

6.TEST SETUP

Devices were biased using a dedicated PCB manufactured by Sodern. The devices in the off state were placed into sockets from which the pins were short circuited.

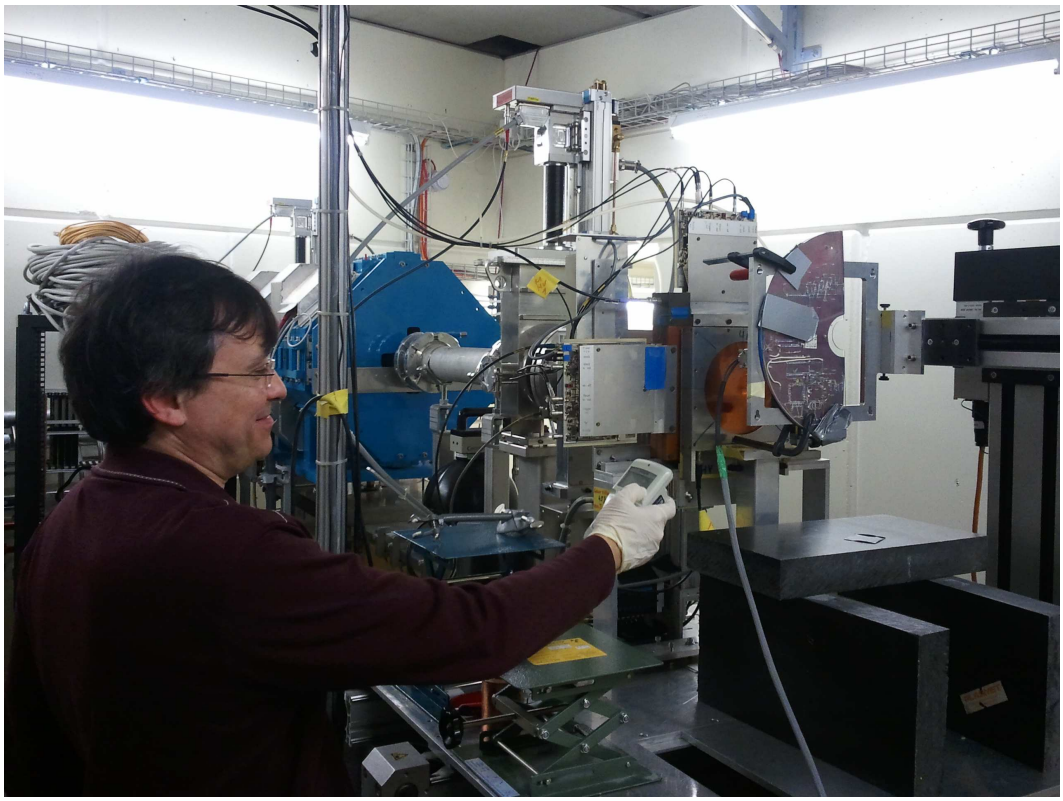

Figure 6-1: Proton DDD setup

7.Test Plan

Electrical and electro-optical measurements are performed at the following steps:

- Initial characterization
- 1.00+09/cm^2
- 3.00+09/cm^2
- 1.00+10/cm^2
- 3.00+10/cm^2
- 1.00+11/cm^2
- 5.00+11/cm^2
- 8 months room temperature annealing (no measurements)
- 2 weeks 50 degC annealing (measurements twice a week)
- 168 hours 125 degC annealing (3 measurements in 7 days)

Please note that the actual radiation levels are different from the ones in the test plan. This was mainly due to the restricted amount of radiation beam time we had available.

Due to time constraints and un-availability of the parts electro optical testing is not performed after proton testing.

Devices have been irradiated using the following bias conditions:

Proton Energy	Bias State during Irradiation test campaign	Bias state during Post irradiation annealing	Serial Numbers
100 MeV	ON	ON	675
100 MeV	ON	ON	677
100 MeV	OFF	OFF	710
100 MeV	OFF	OFF	670
176 MeV	ON	ON	671
176 MeV	ON	ON	711
176 MeV	OFF	OFF	681
176 MeV	OFF	OFF	708
230 MeV	ON	ON	719
230 MeV	ON	ON	674
230 MeV	OFF	OFF	726
230 MeV	OFF	OFF	727

Please note that the annealing bias condition is different as the ones mentioned in the test plan. Devices were put in annealing under the same conditions as during irradiation due to a mistake during test setup.

Electrical testing was performed after the following intermediate irradiation levels:

	100 MeV	176MeV	230 MeV
T0	***	***	***
T1	0.91+10/cm^2	1.13+10/cm^2	1.23+10/cm^2
T2	3.04+10/cm^2	3.75+10/cm^2	4.11+10/cm^2
T3	9.12+10/cm^2	1.13+11/cm^2	1.23+11/cm^2
T4	3.04+11/cm^2	3.75+11/cm^2	4.11+11/cm^2
T5	1.52+12/cm^2	1.88+12/cm^2	2.06+12/cm^2

8.EXPERIMENTAL RESULTS

8.1.Reported parameters

The following electrical parameters are reported in the next paragraphs:

- Temporal noise in DR mode (hard reset, hard to soft reset)
- Temporal noise in NDR mode (hard reset, hard to soft reset)
- Offsets (in particular DR mode odd/even offset difference and NDR mode offset dispersion – mean, standard deviation, register value)
- Fixed pattern noise (FPN) local and global (hard reset, hard to soft reset)
- Dark current
- Dark current non uniformity local and global
- Photo response non uniformity local and global
- Temperature sensor output
- Supply currents
- ADC Performances (INL, DNL)

8.2.Observations

The electrical test during annealing is performed with the new HAS2 production tester as the old one was not available anymore due to a failure inside the electronics which could not be fixed (root cause of the failure could not be traced). As there are some differences between the two testers, results of both testers are kept apart from each other.

During annealing, some strange behavior has been noticed in the dark current images in NDR (clearly visible in both R and S images). The same behavior is seen in the dark short images in DR mode (enhanced levels and only in soft rest mode).

During the high temperature anneal the effect remained.

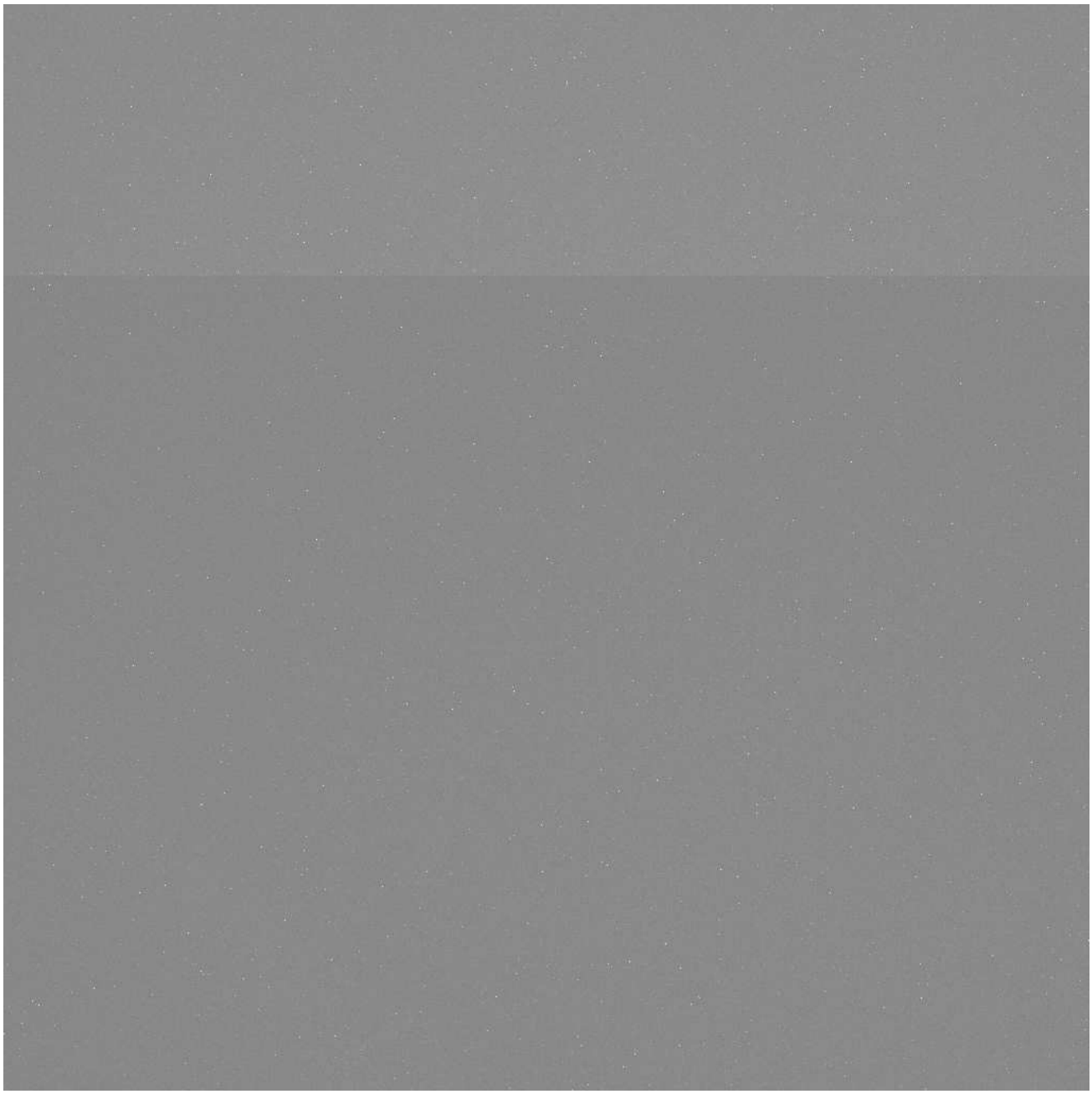

Figure 8-1 : Sample 674 Reset NDR image

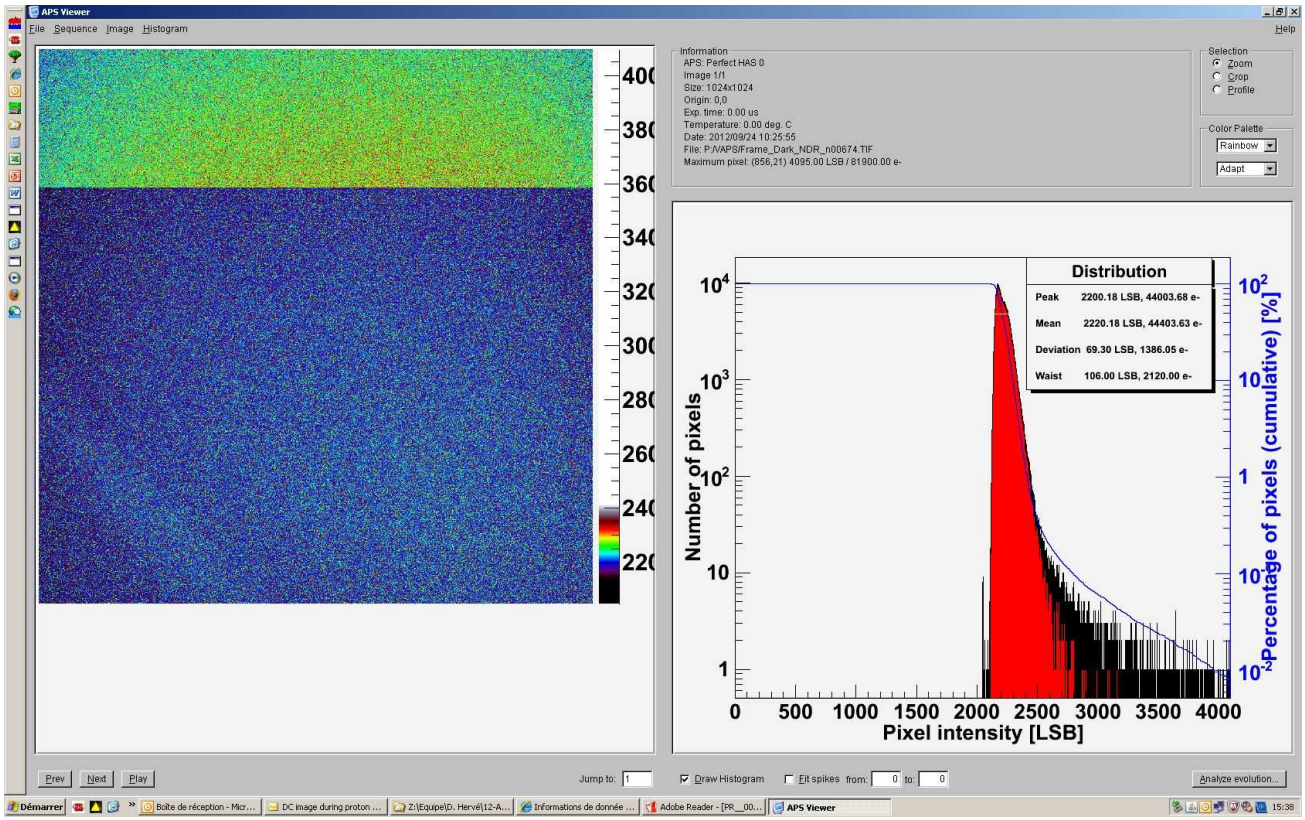

Figure 8-2: Analysis of sample 674 Reset NDR image

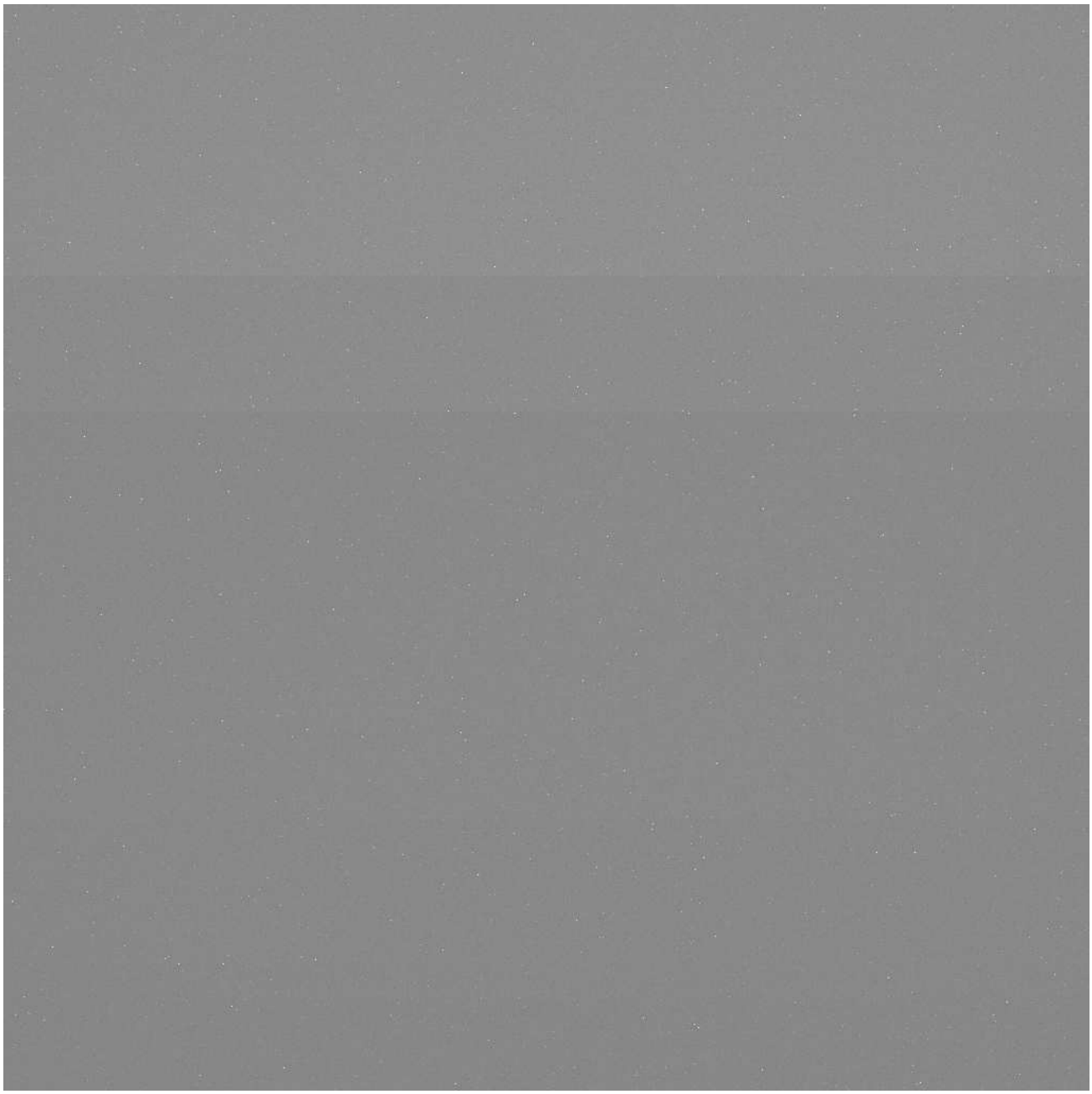

Figure 8-3: Sample 671 Reset NDR image

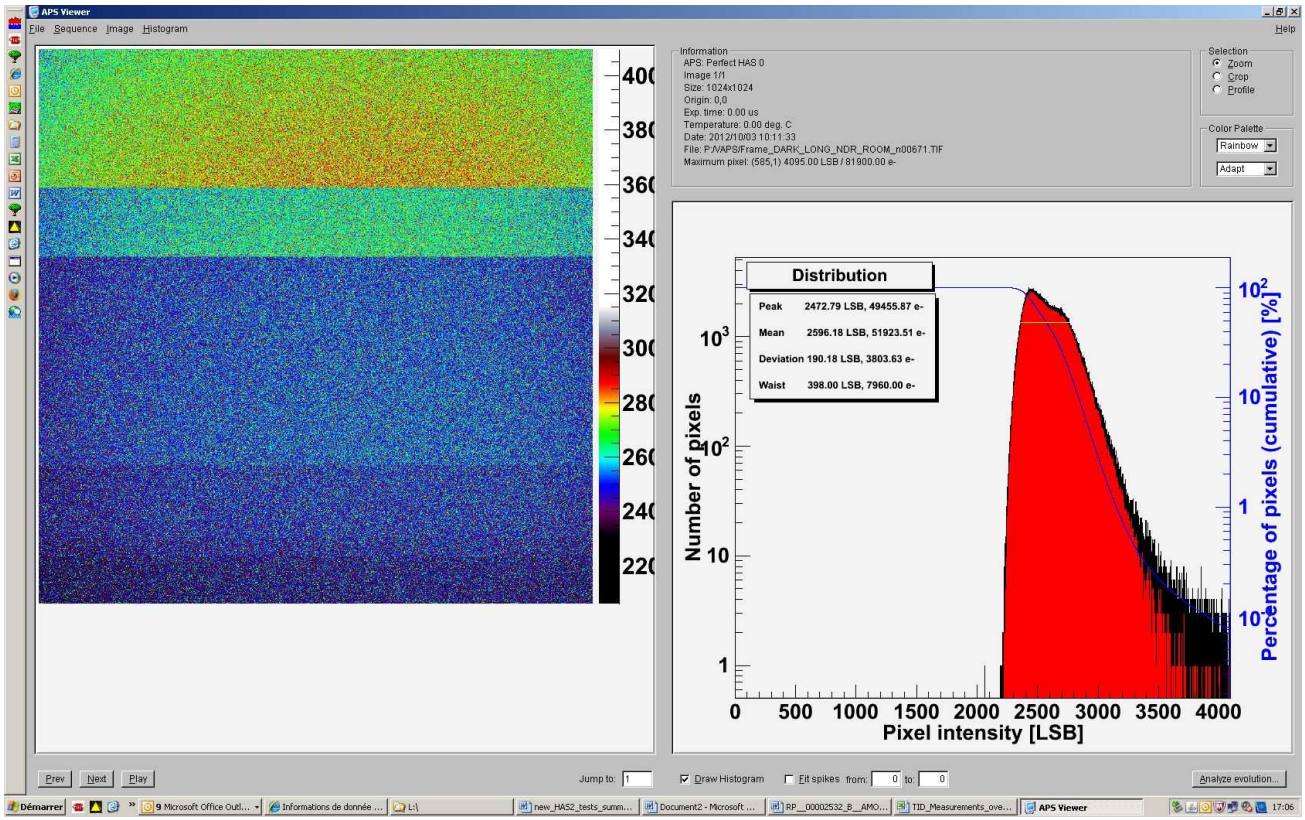

Figure 8-4: Analysis of sample 671 Reset NDR image

8.2.1.Dark Current

8.2.1.1.During irradiation

The following graph is displaying the average dark current behavior of the 8 different biasing conditions.

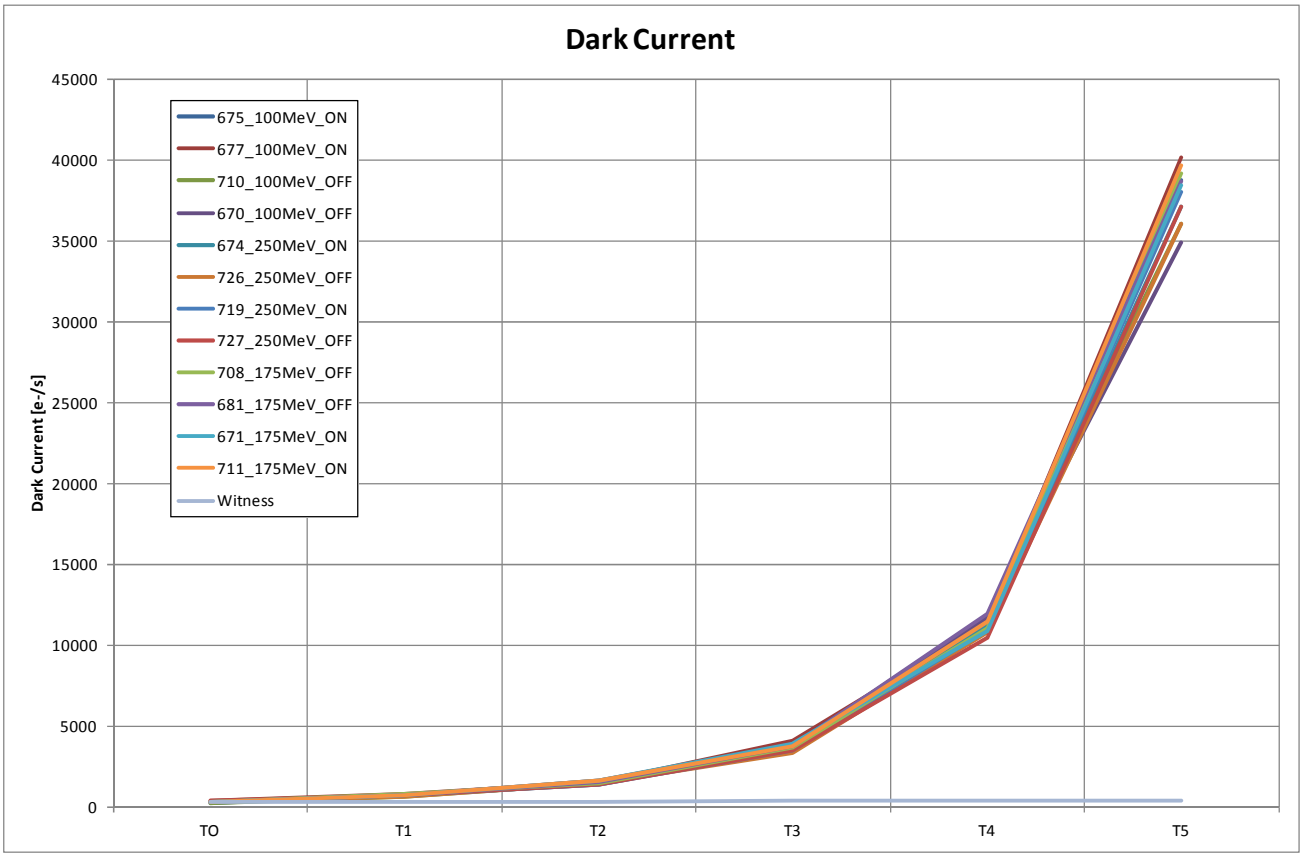

Figure 8-5: Dark Current vs radiation for different proton energies

The following observations are made:

- Dark current increases the same for all the samples, independent from the biasing conditions, independent from the energy.

The graph below is showing the DSNU distributions for device ID 681 which was in the OFF state during radiation and annealing. Please note that the below curves have an integration time of 1 second.

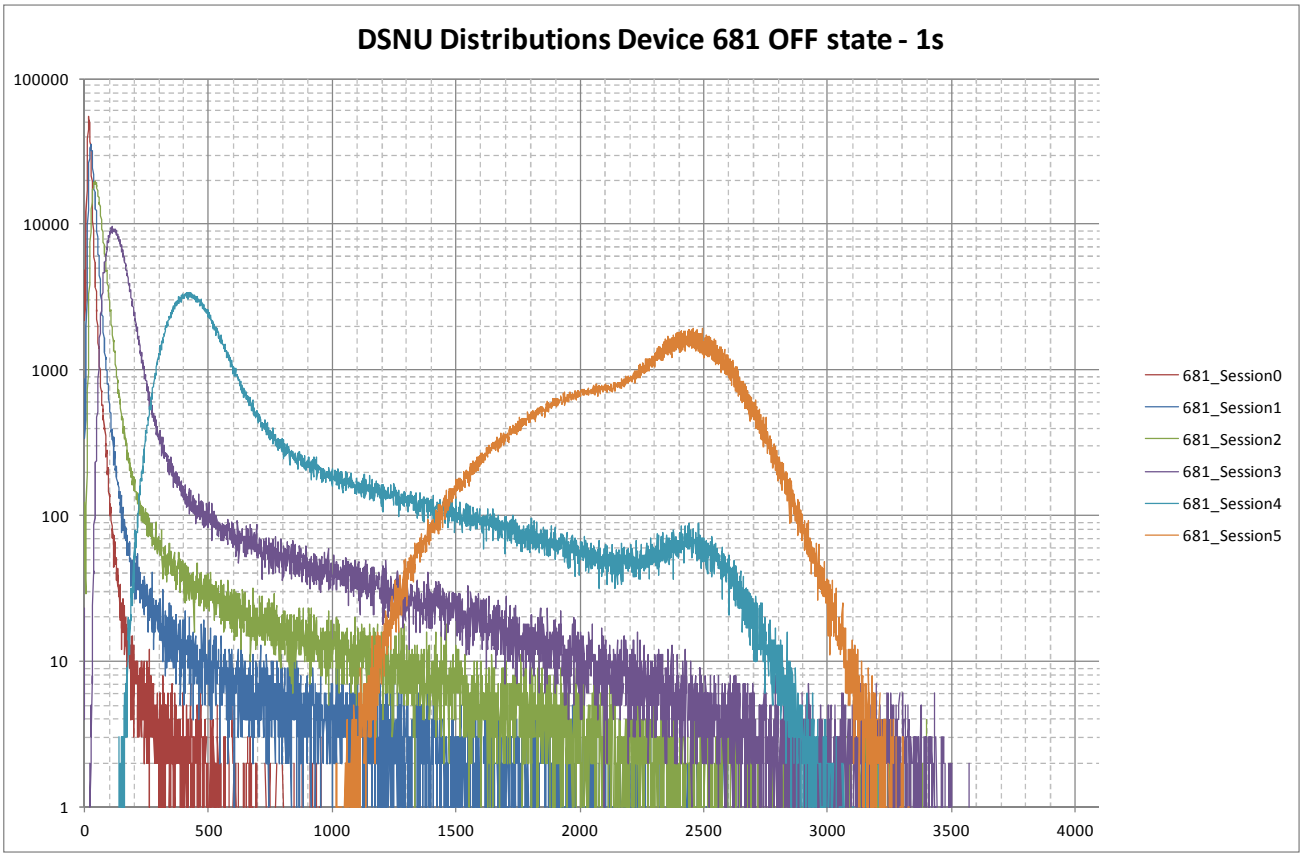

Figure 8-6: DSNU distributions 1s during radiation for device 681

⇨ Some saturated pixels are visible in the histogram and will lead to a wrong interpretation of the dark current. In order to obtain the correct dark current, the dark short image is used (next page).

The next graph is showing the DSNU distributions for the NDR dark short image which have an integration time of 167ms.

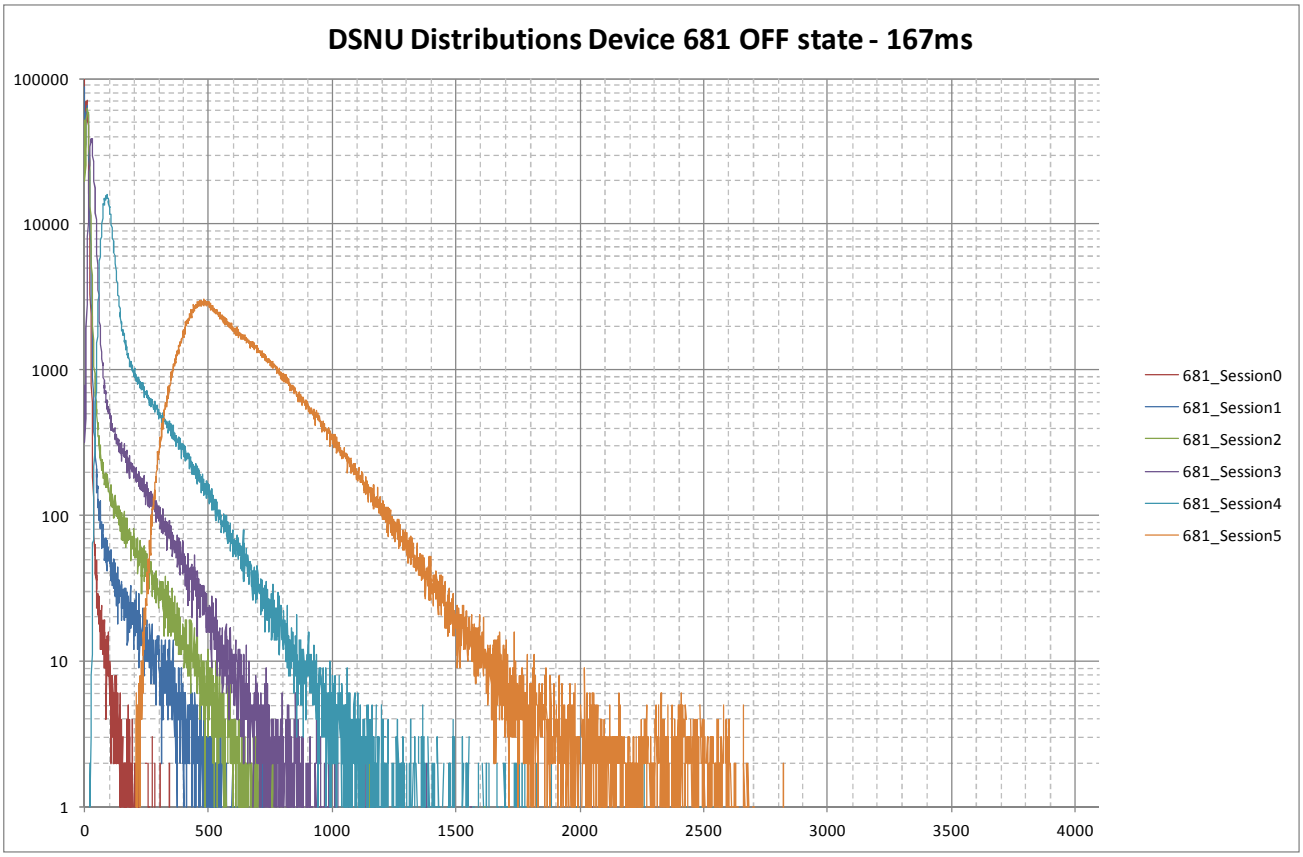

Figure 8-7: DSNU distributions 167ms during radiation for device 681

The graph below is showing the DSNU distributions for device ID 711 which was in the OFF state during radiation and annealing. Please note that the below curves have an integration time of 1 second.

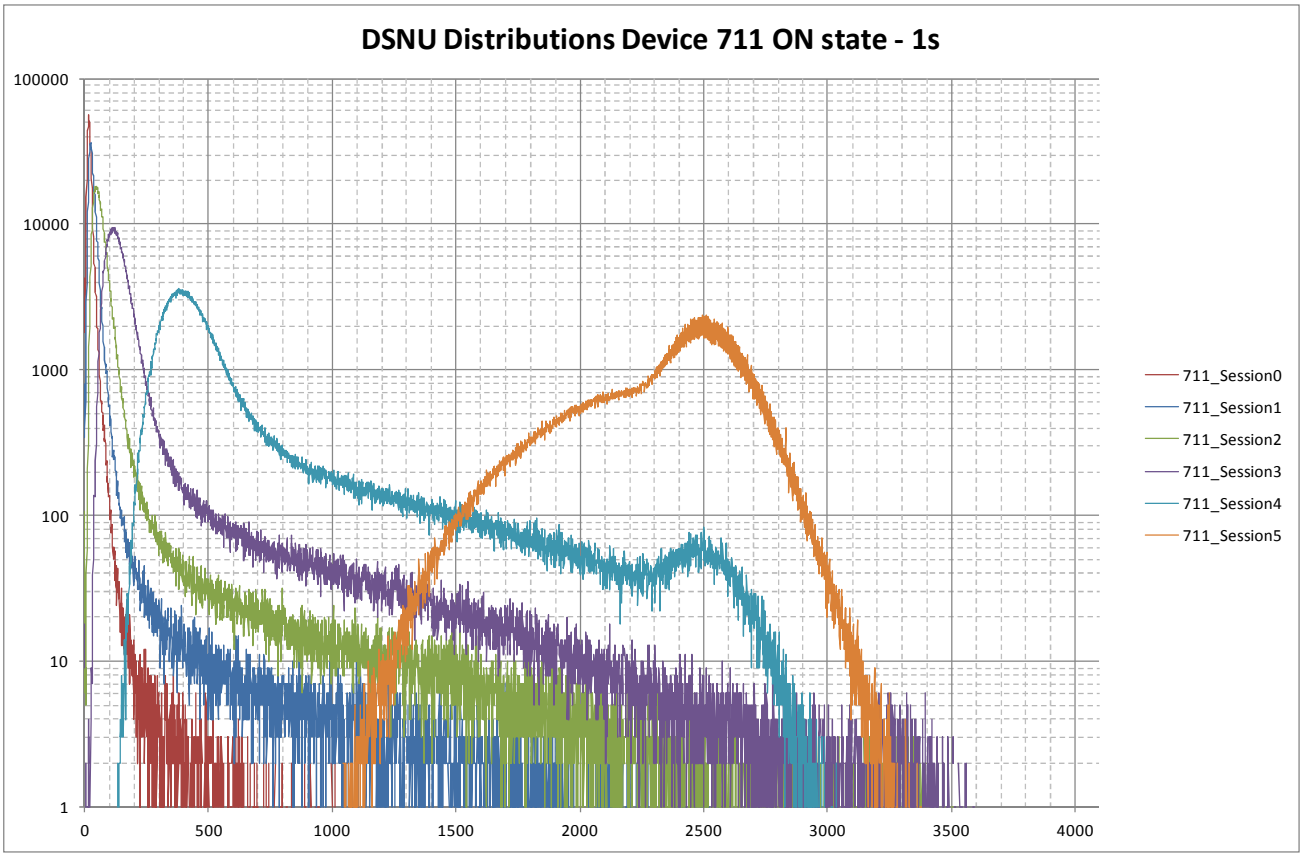

Figure 8-8: DSNU distributions 1s during radiation for device 711

⇨ Some saturated pixels are visible in the histogram and will lead to a wrong interpretation of the dark current. In order to obtain the correct dark current, the dark short image is used (next page).

The next graph is showing the DSNU distributions for the NDR dark short image which have an integration time of 167ms.

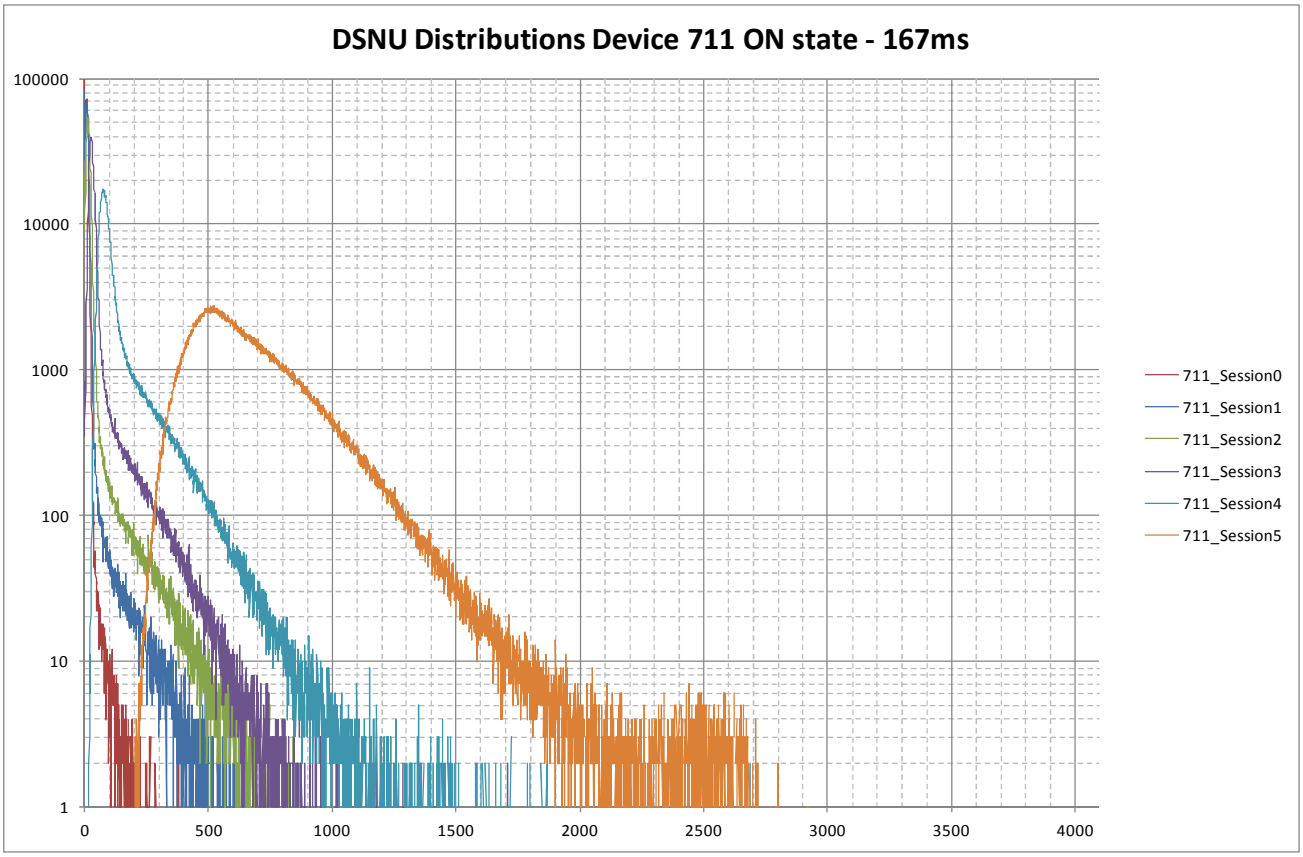

Figure 8-9: DSNU distributions 167ms during radiation for device 711

8.2.1.2.During Annealing

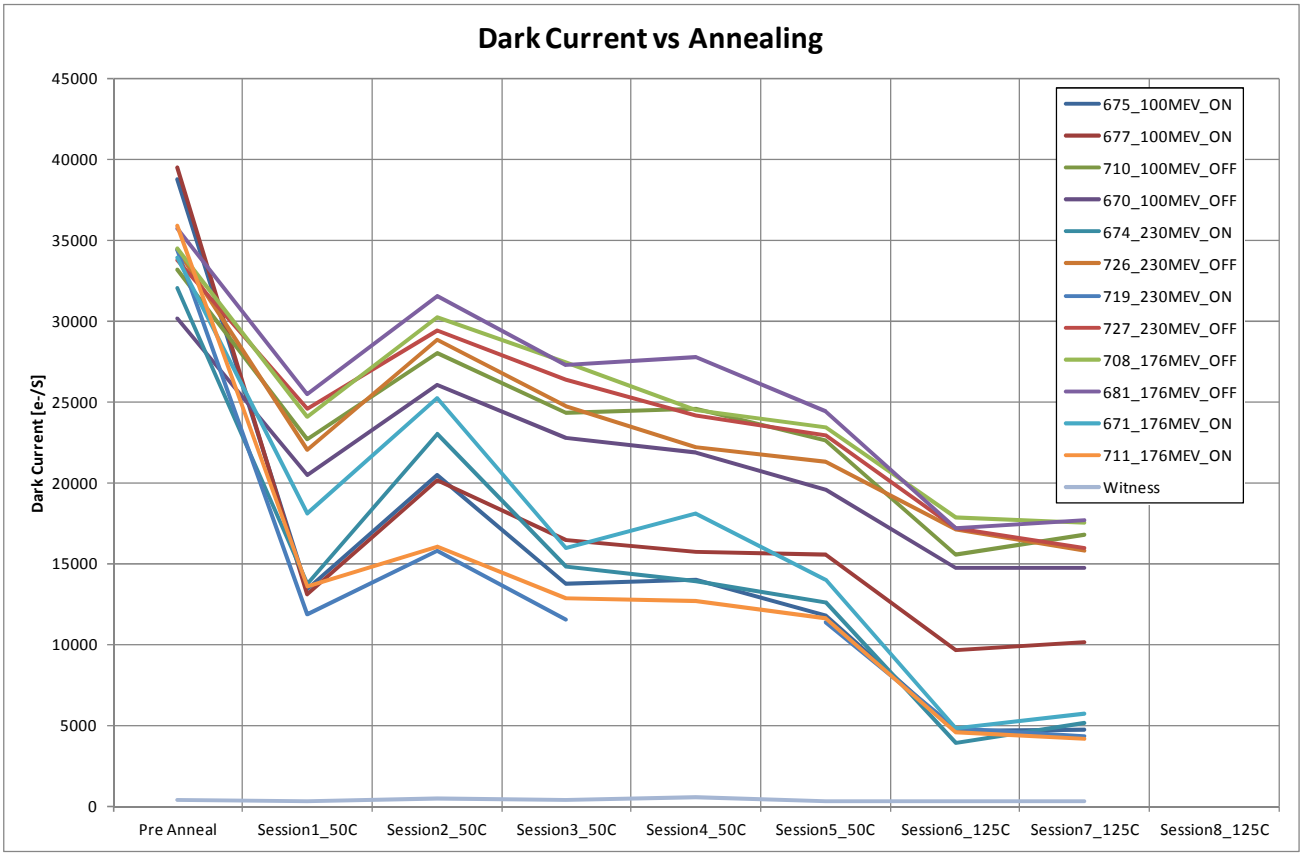

Figure 8-10: Dark Current vs annealing for different proton energies

The following observations are made:

- Dark current decreases faster for the samples in the ON state.
- The unstable behavior is due to the fact that the parts are not tested with a thermo stream.
- The decrease of dark current is stopping already after 1 day of 125C annealing.

The next graph is also showing the DSNU distributions for device 681 but this time after room temperature, 50C and 125C annealing. For these distributions an integration time of 1 second was applied.

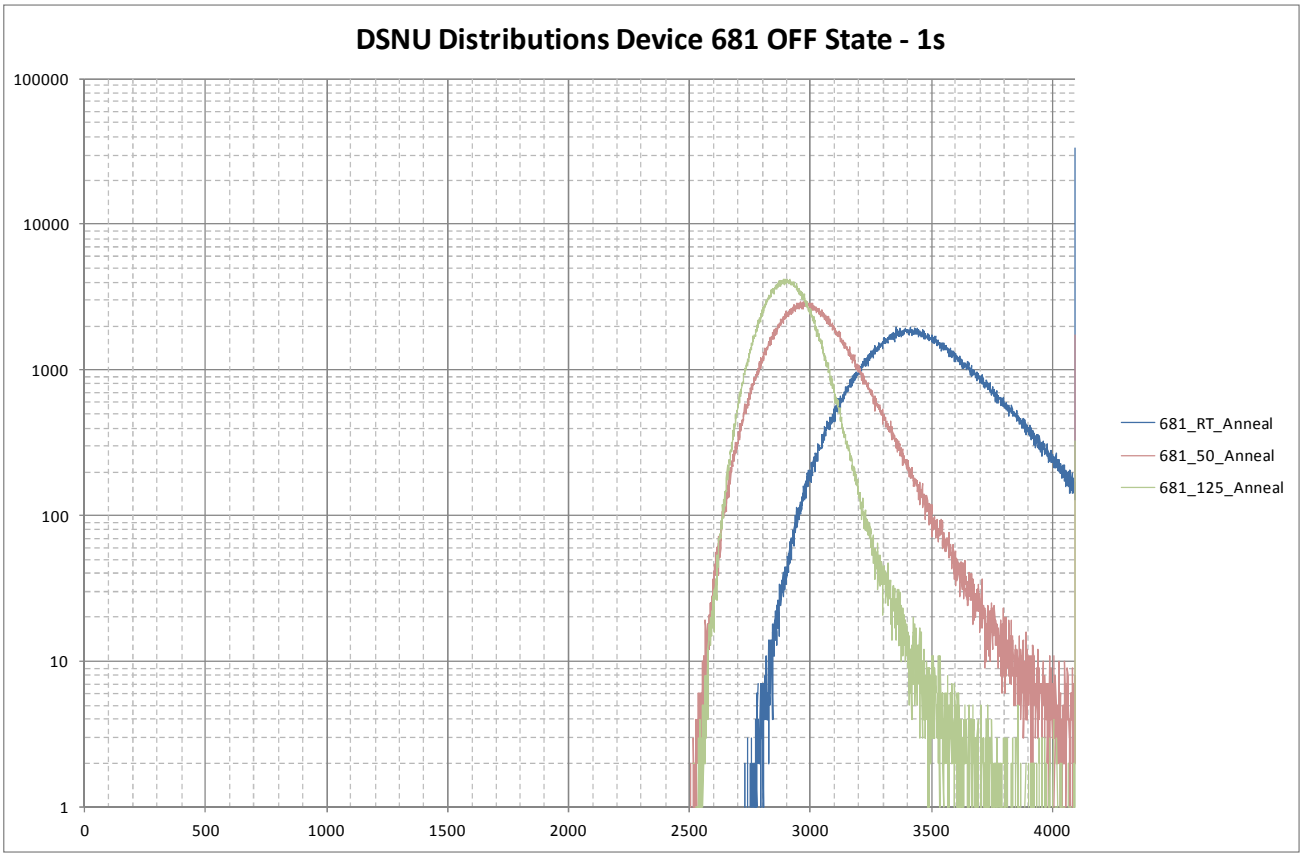

Figure 8-11: DSNU distributions 1s during annealing for device 681

The next graph is showing the DSNU distributions for the NDR dark short image which have an integration time of 167ms.

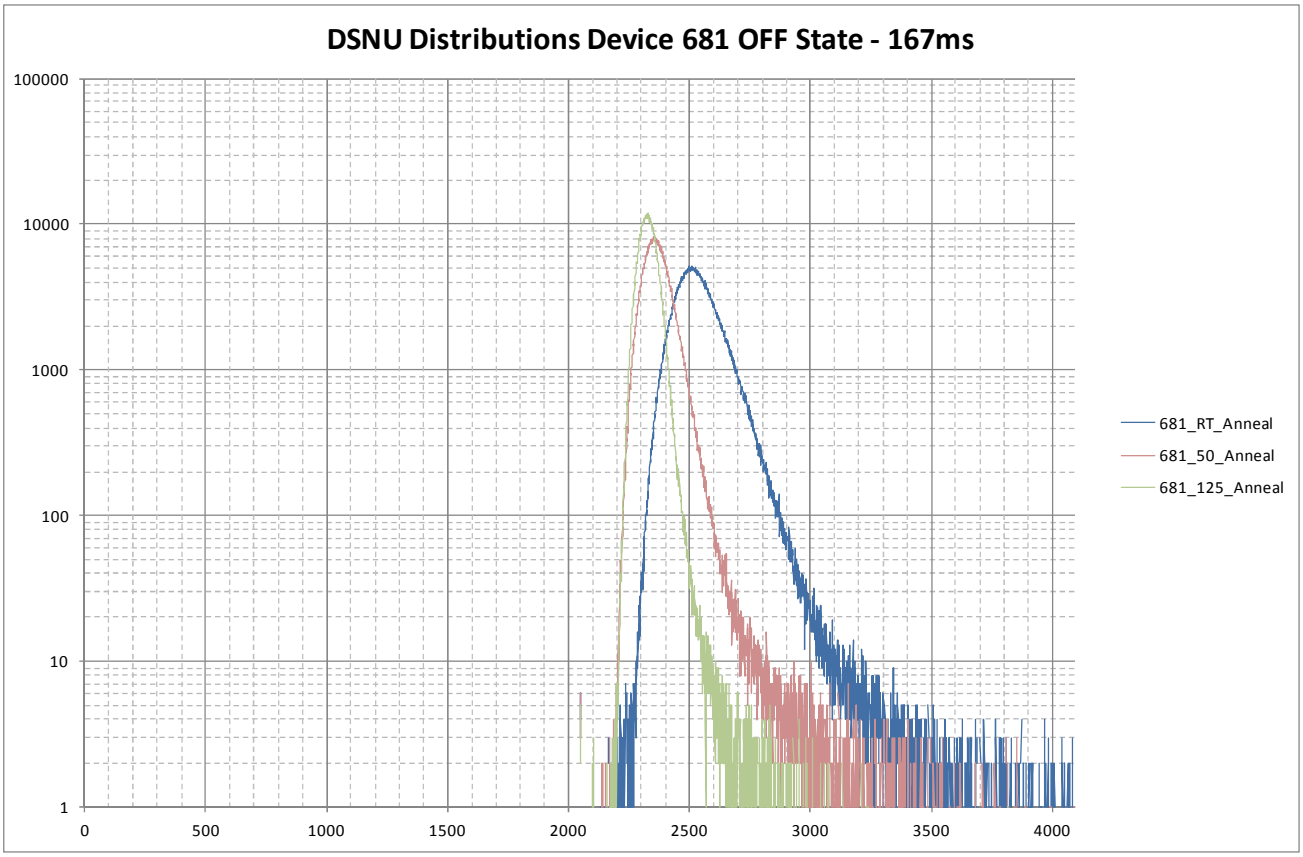

Figure 8-12: DSNU distributions 167ms during annealing for device 681

The next graph is also showing the DSNU distributions for device 711 but this time after room temperature, 50C and 125C annealing. For these distributions an integration time of 1 second was applied.

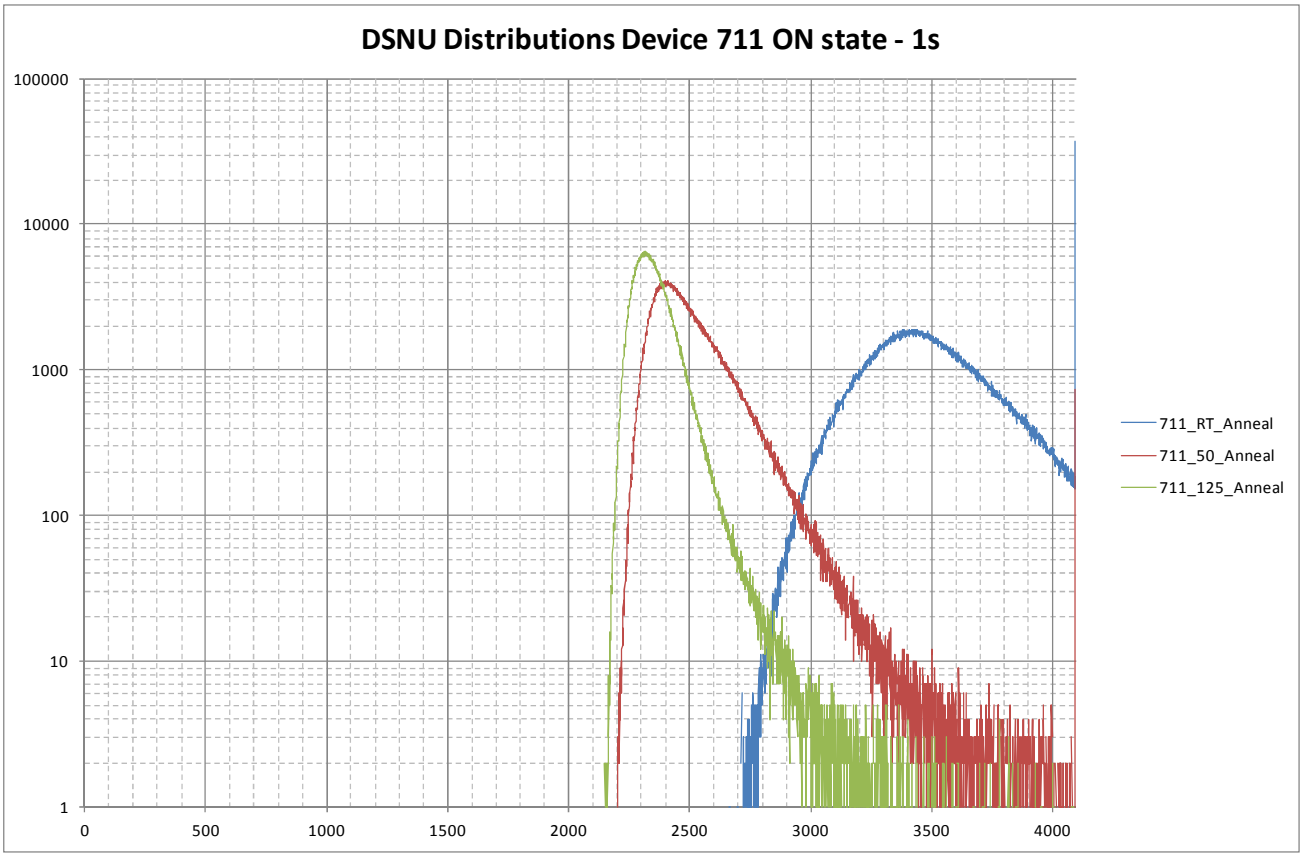

Figure 8-13: DSNU distributions 1s during annealing for device 711

The next graph is showing the DSNU distributions for the NDR dark short image which have an integration time of 167ms.

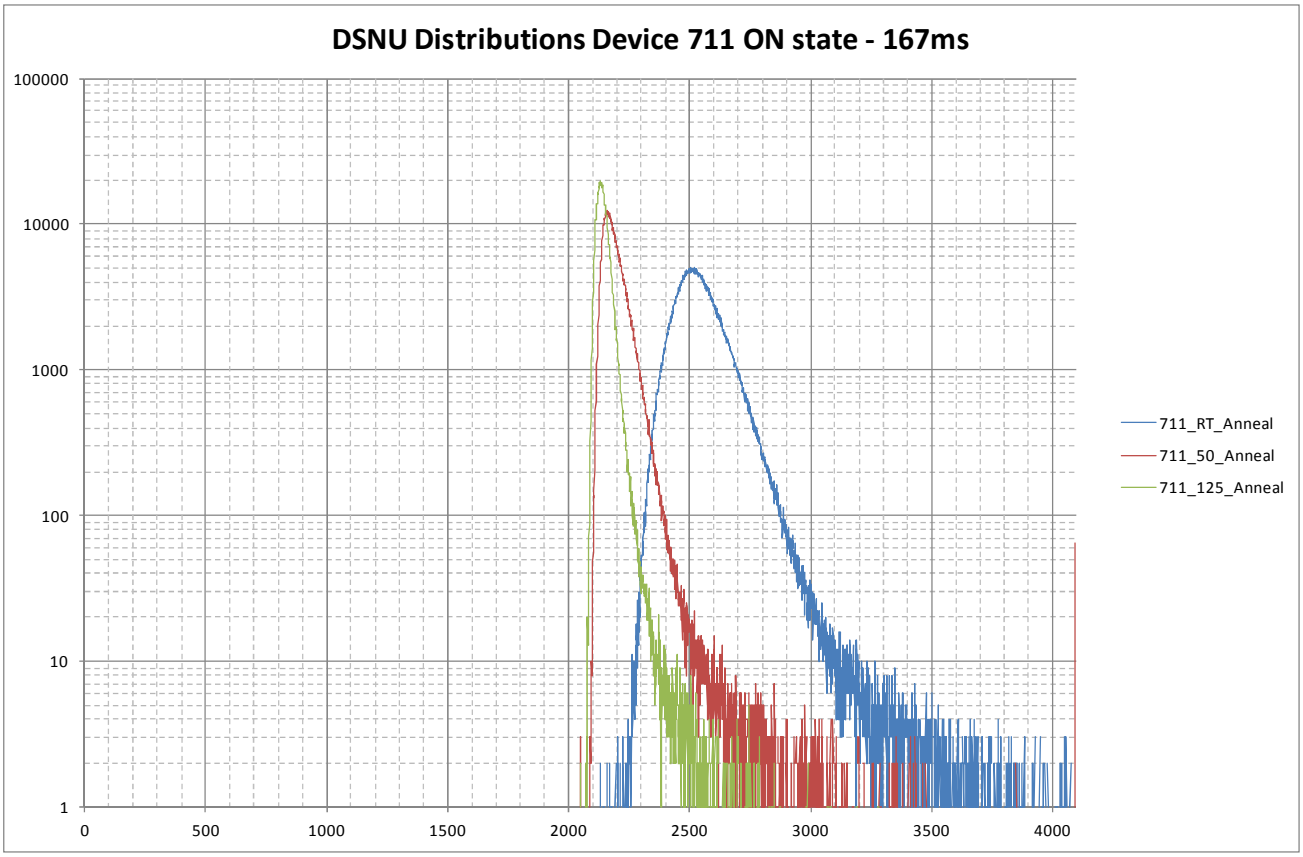

Figure 8-14: DSNU distributions 167ms during annealing for device 711

8.2.2.Temporal Noise in DR Mode – hard reset

8.2.2.1.During Irradiation

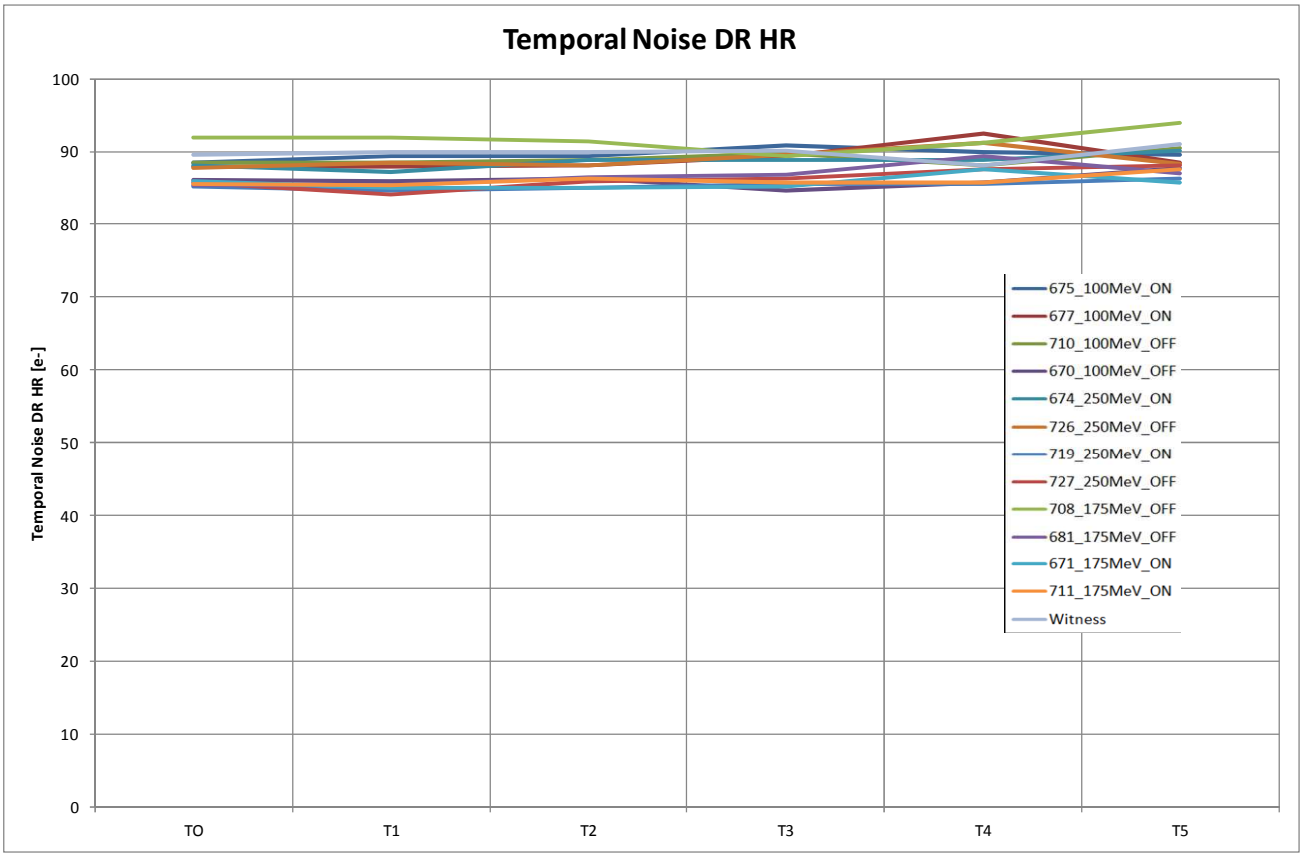

Figure 8-15: Temporal Noise in DR mode – hard reset vs radiation for different proton energies

The following observations are made:

- Temporal noise is not affected by the energy nor the bias condition.

8.2.2.2.During Annealing

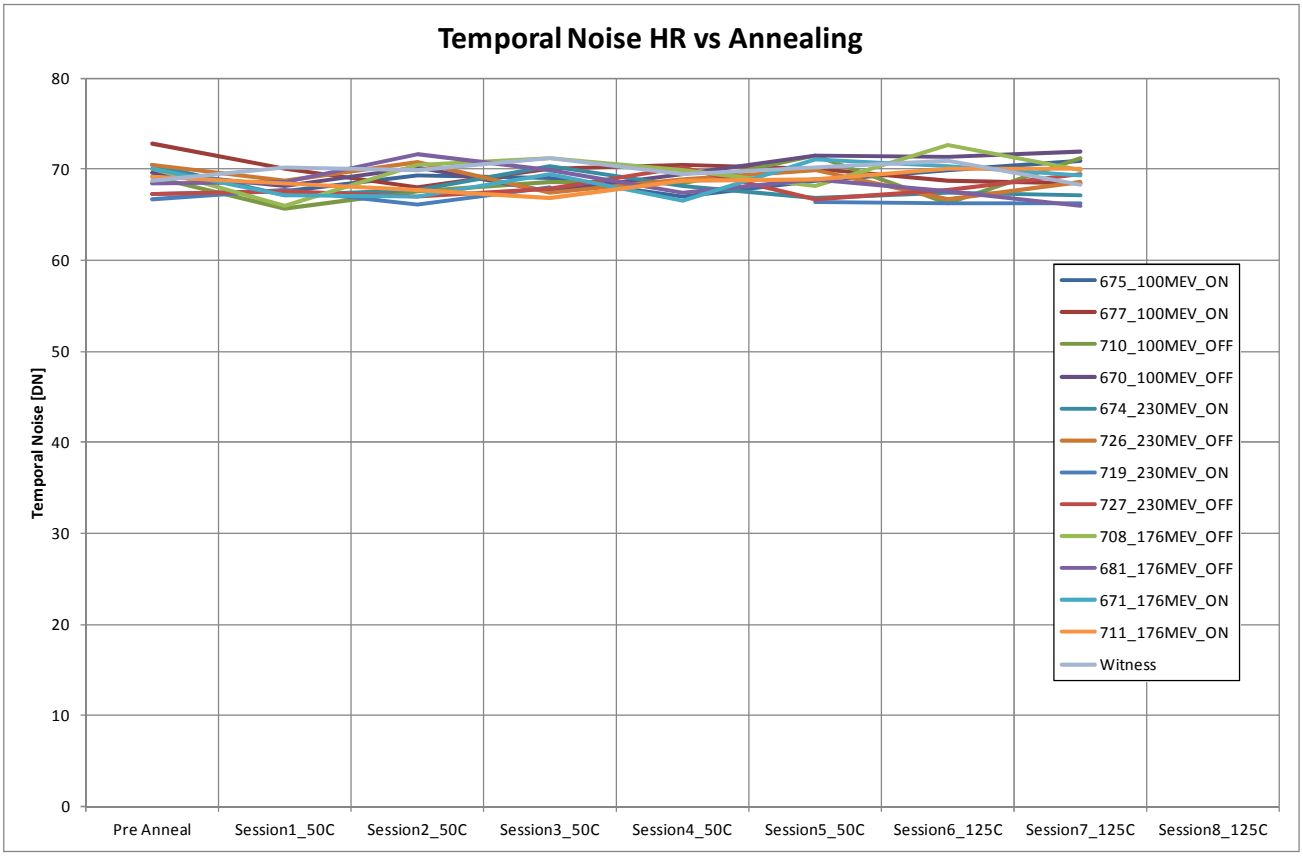

Figure 8-16: Temporal Noise in DR mode – hard reset vs annealing for different proton energies

The following observations are made:

- Temporal noise is not affected by the annealing or the bias condition.
- Please note the temporal noise measured on the new test system is much lower (better test system – more stable supplies).

8.2.3.Temporal Noise in DR Mode – hard to soft reset

8.2.3.1.During Radiation

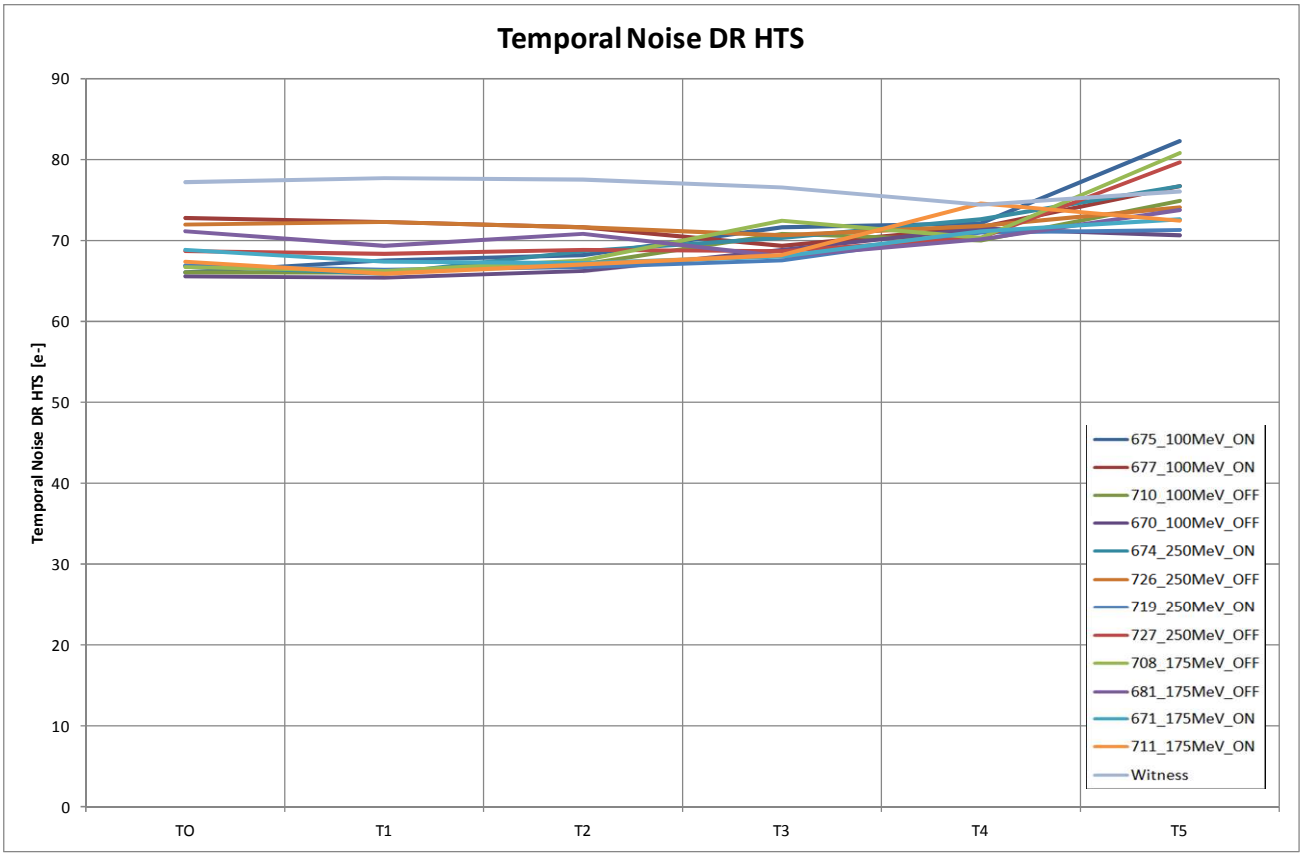

Figure 8-17: Temporal Noise in DR mode – hard to soft reset vs radiation for different proton energies

The following observations are made:

- Temporal noise is slightly increasing after T4 and T5.
- Temporal noise behavior is the same for all parts independent from the biasing and energy.

8.2.3.2.During Annealing

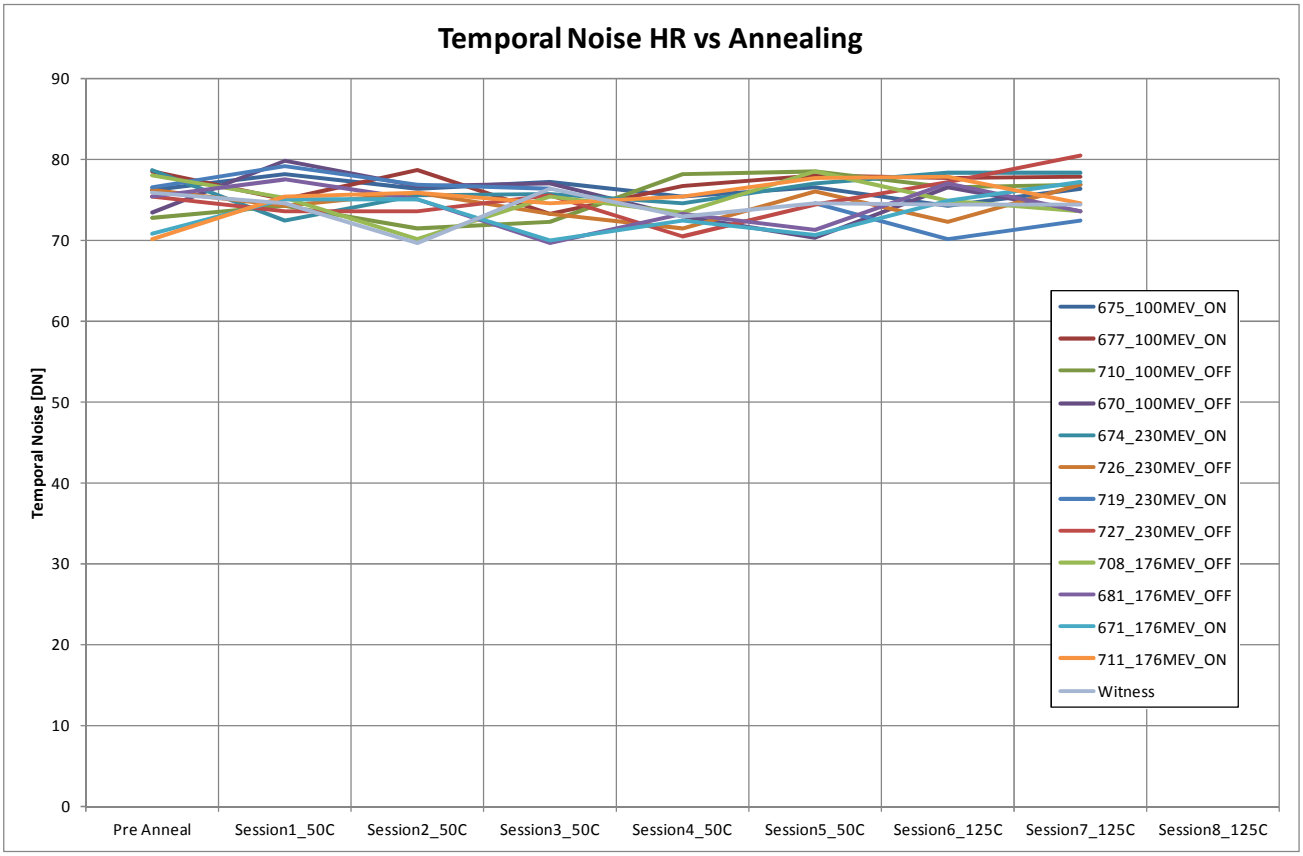

Figure 8-18: Temporal Noise in DR mode – hard to soft reset vs annealing for different proton energies

The following observations are made:

- Temporal noise is not affected by the annealing or the bias condition.

8.2.4. Temporal Noise in NDR Mode – hard reset

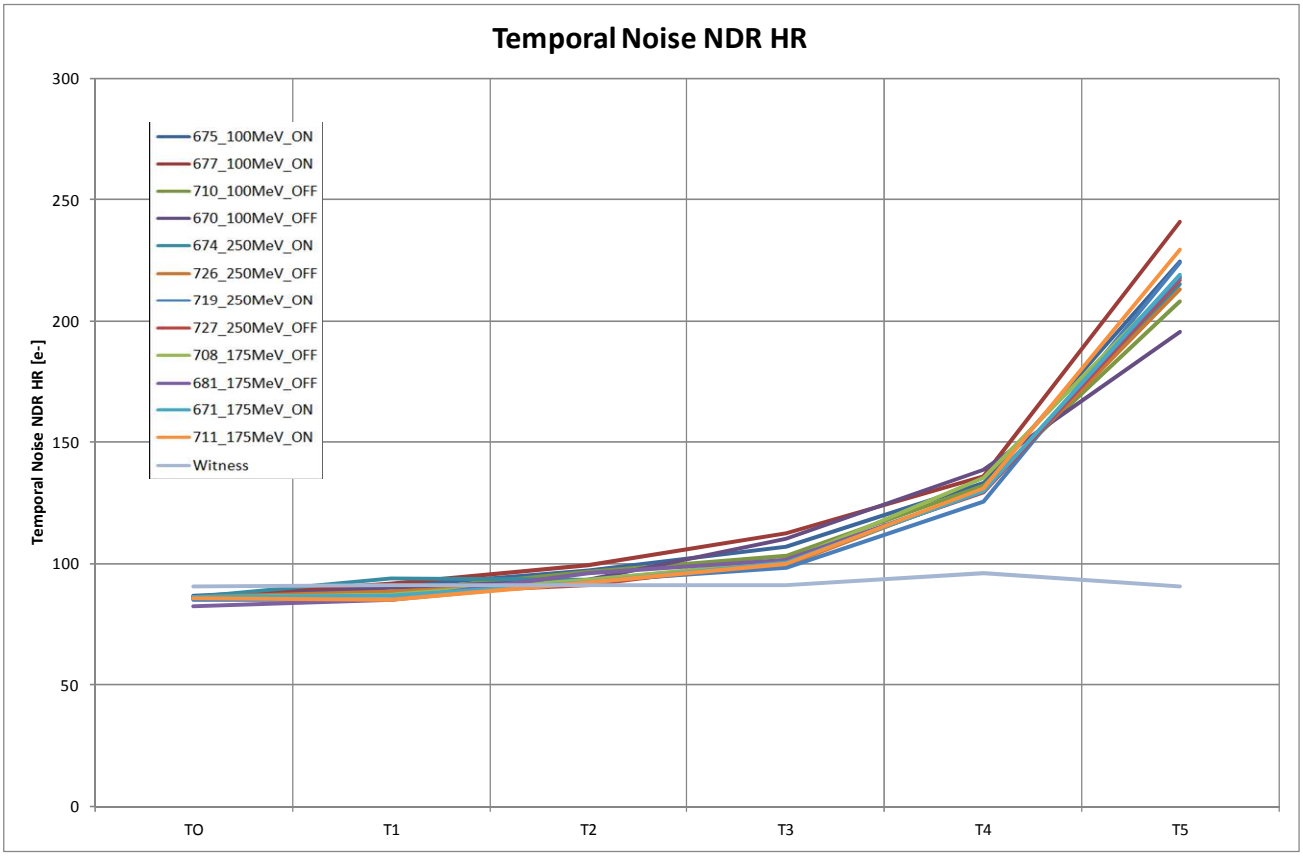

Figure 8-19: Temporal Noise in NDR mode – hard reset vs radiation for different proton energies

The following observations are made:

- Temporal noise is increasing with radiation. This is probably due to the 200ms minimal integration time on the tester. With increasing radiation a dark current component is added to the temporal noise. There is no difference in biasing scheme nor energy level.

8.2.5. Temporal Noise in NDR Mode – hard to soft reset

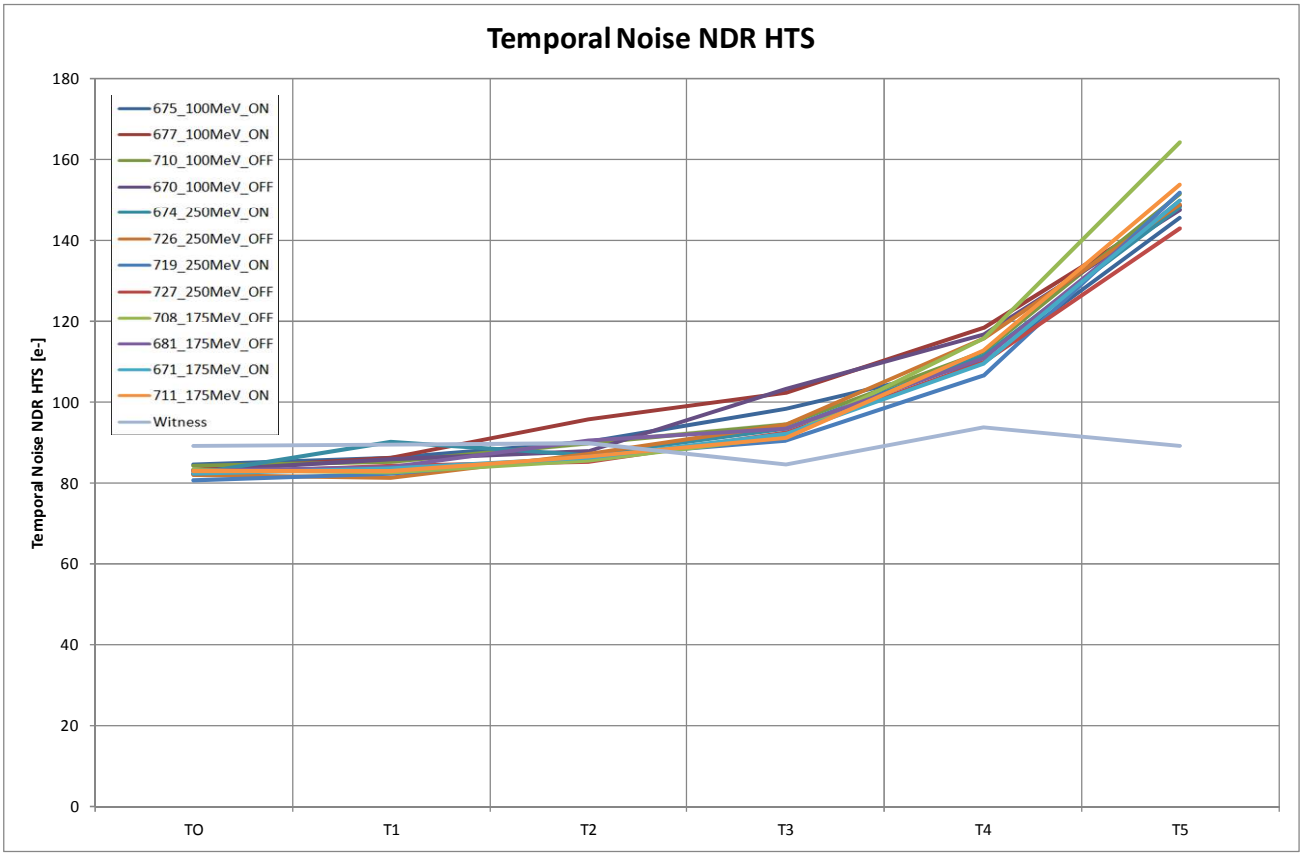

Figure 8-20: Temporal Noise in NDR mode – hard to soft reset vs radiation for different proton energies

The following observations are made:

- Temporal noise is increasing with radiation. This is probably due to the 200ms minimal integration time on the tester. With increasing radiation a dark current component is added to the temporal noise. There is no difference in biasing scheme.

8.2.6.Global Fixed Pattern Noise – hard reset

8.2.6.1.During Radiation

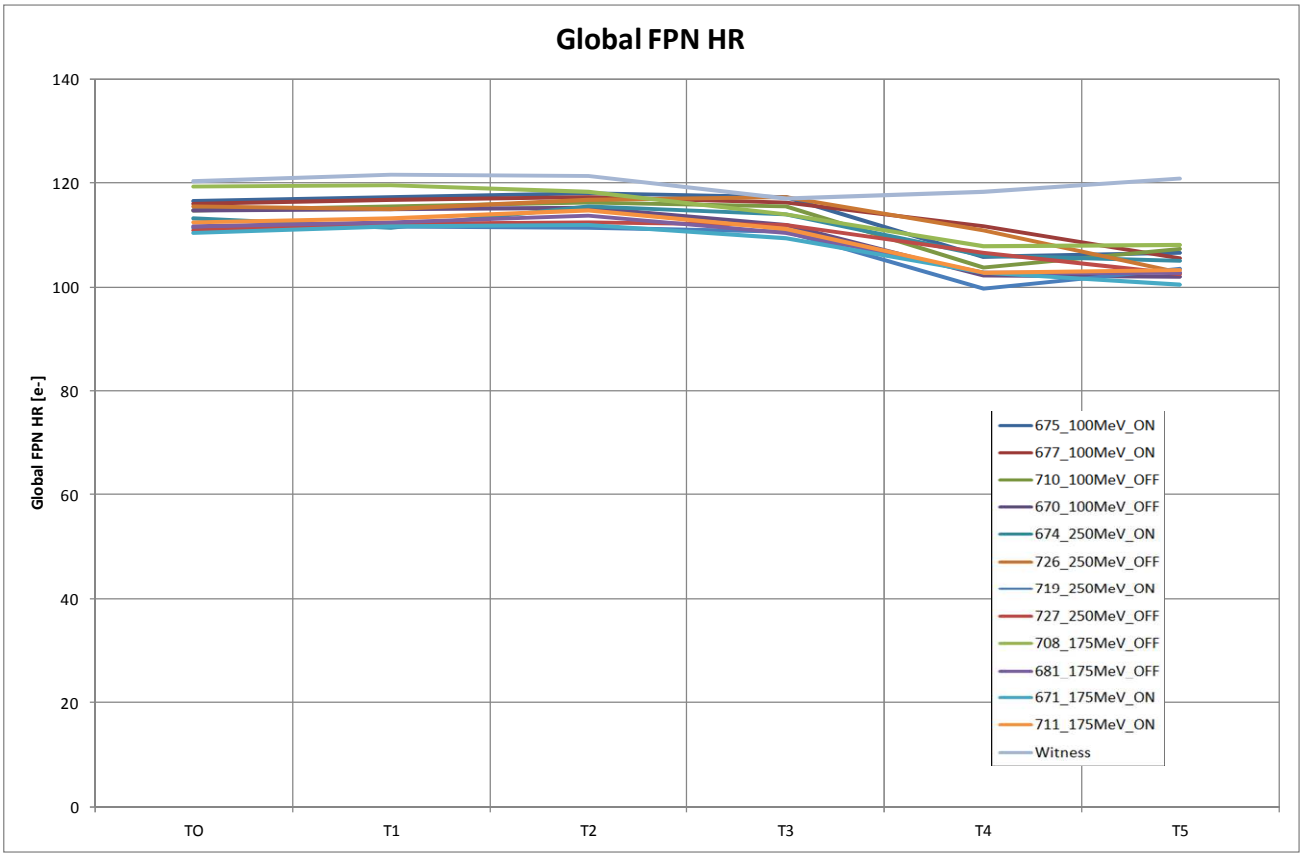

Figure 8-21: Global FPN – hard reset vs radiation for different proton energies

The following observations are made:

- FPN is decreasing during the T4 radiation sessions to be stable again during the T5 radiation session.
- There is no difference amongst the bias settings or proton energies.

8.2.6.2.During Annealing

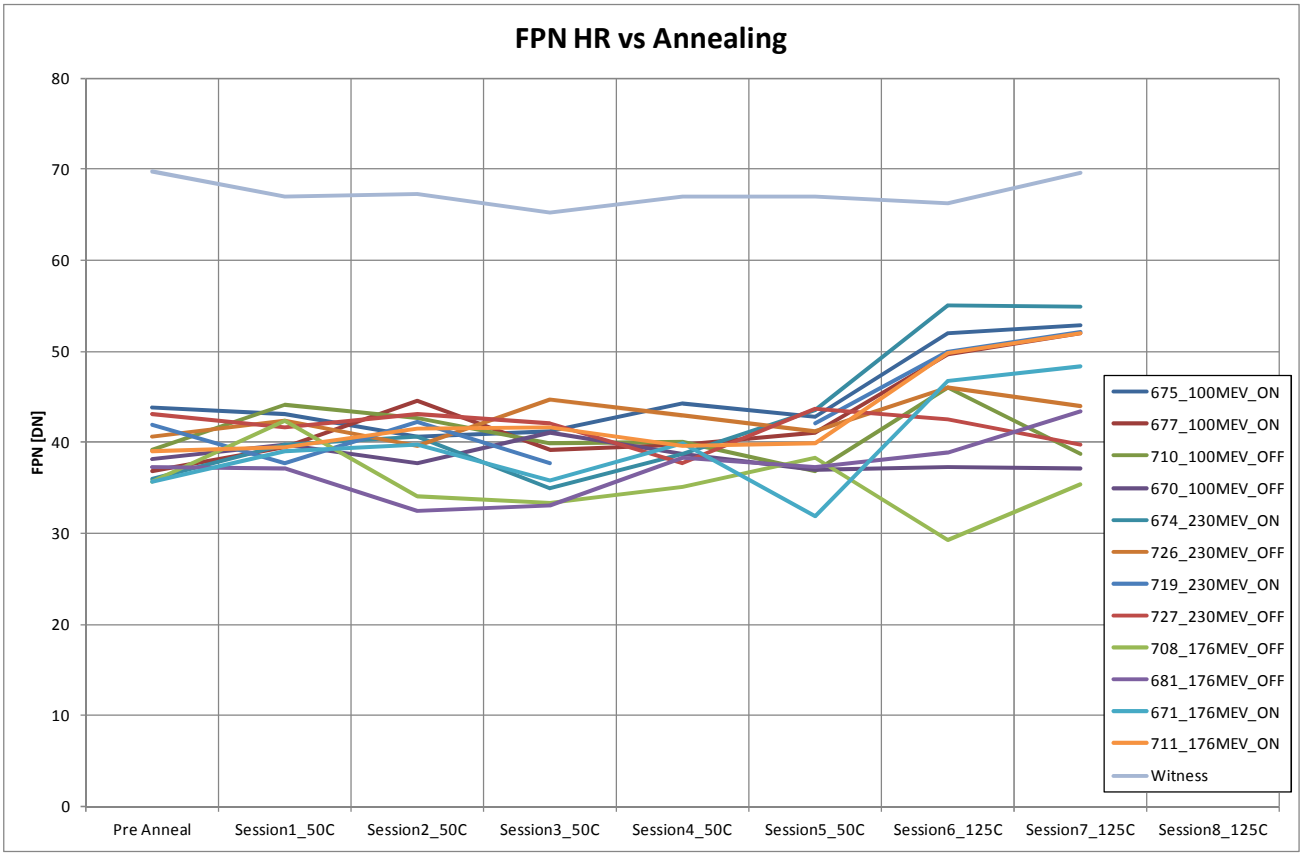

Figure 8-22: Global FPN – hard reset vs annealing for different proton energies

The following observations are made:

- FPN is not affected by the annealing or the bias condition during 50C annealing.
- FPN is slightly increasing during the 125C annealing for those devices in the ON state.
- Please note the FPN measured on the new test system is much lower (better test system – more stable supplies).

8.2.7.Global Fixed Pattern Noise – hard to soft reset

8.2.7.1.During Radiation

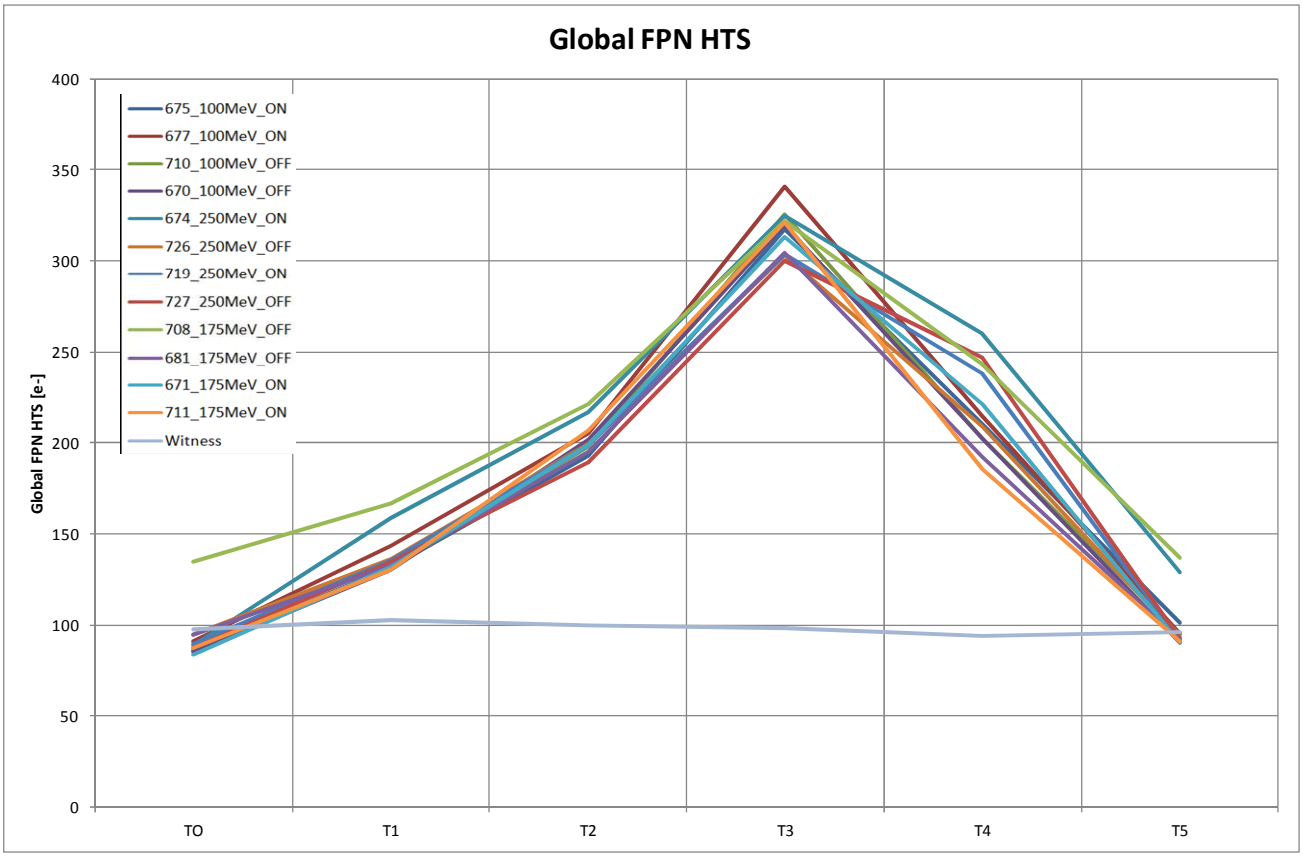

Figure 8-23 Global FPN – hard to soft reset vs radiation for different proton energies

The following observations are made:

- FPN is increasing significantly during the first 3 irradiation sessions, to come back to it's initial value during T4 and T5 irradiation sessions. This phenomenon was also observed during the neutron testing (other location, other date). The reason for this behavior is unknown but is most likely related to the driving electronics of the hard to soft reset.

- There is no difference amongst the bias settings or proton energies.

8.2.7.2.During Annealing

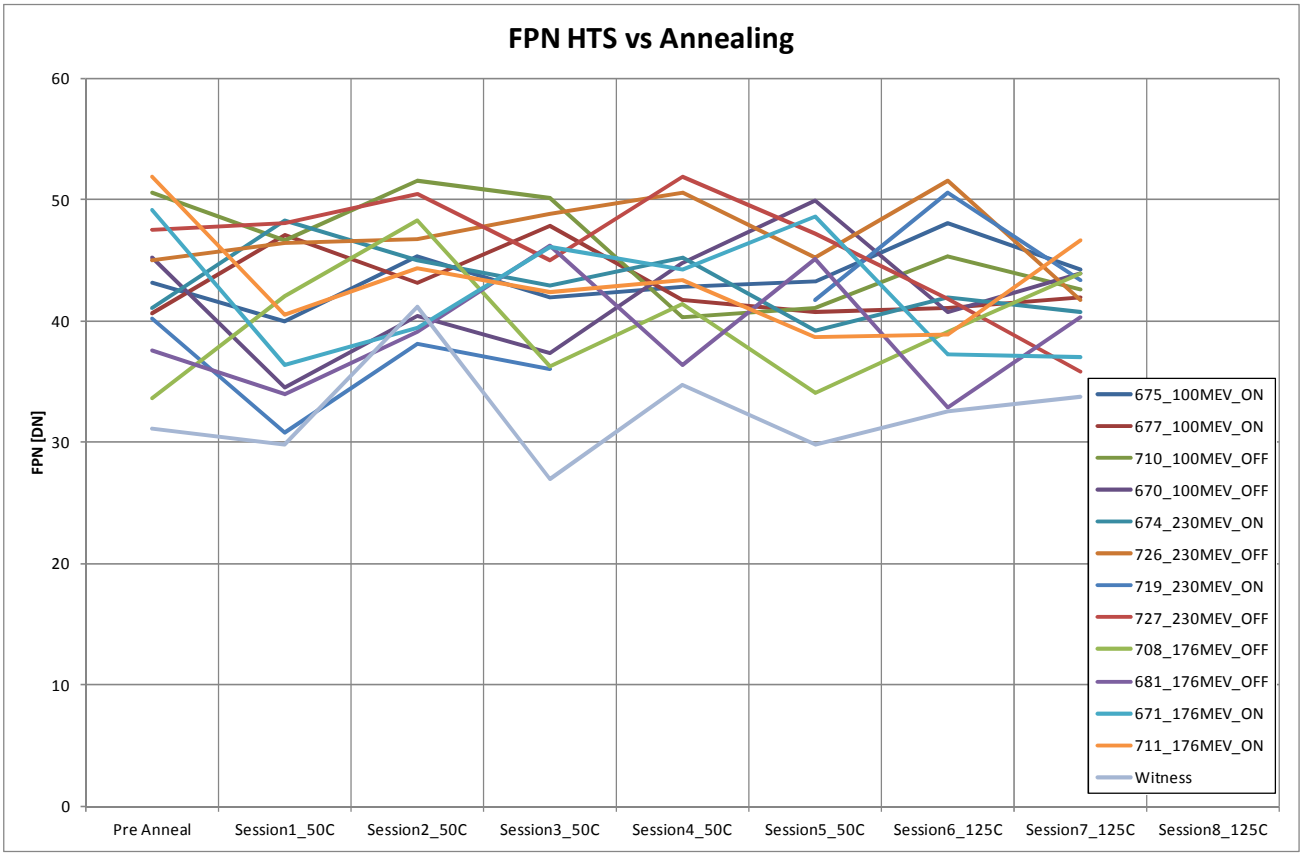

Figure 8-24 Global FPN – hard to soft reset vs annealing for different proton energies

The following observations are made:

- FPN is not affected by the annealing or the bias condition.
- Please note the FPN measured on the new test system is much lower (better test system – more stable supplies).

8.2.8.Local Fixed Pattern Noise – hard reset

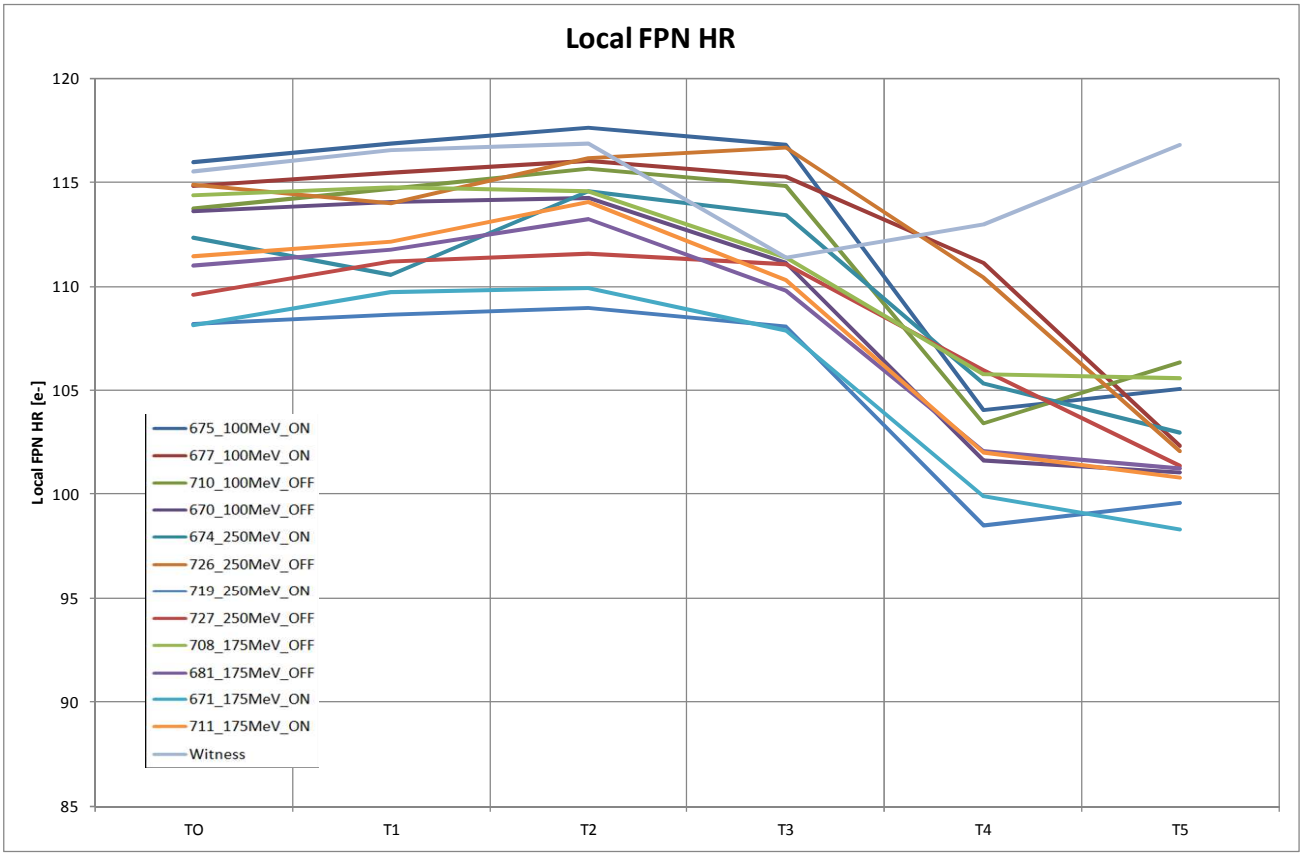

Figure 8-25 Local FPN – hard reset vs radiation for different proton energies

The following observations are made:

- FPN is decreasing during the T4 radiation sessions to be stable again during the T5 radiation session.

- There is no difference amongst the bias settings or proton energies.

8.2.9.Local Fixed Pattern Noise – hard to soft reset

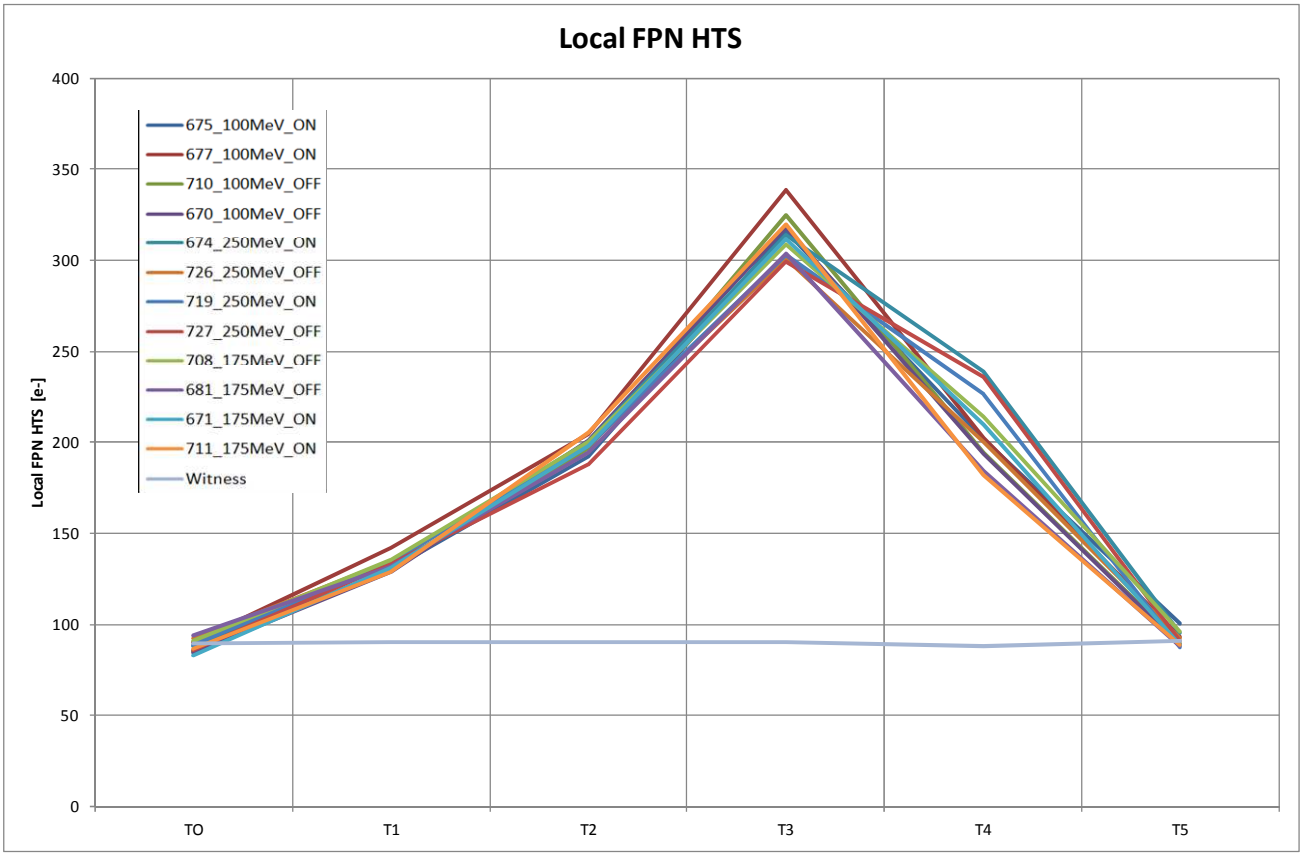

Figure 8-26: Local FPN – hard to soft reset vs radiation for different proton energies

The following observations are made:

- FPN is increasing significantly during the first 3 irradiation sessions, to come back to it's initial value during T4 and T5 irradiation sessions. This phenomenon was also observed during the neutron testing (other location, other date). The reason for this behavior is unknown but is most likely related to the driving electronics of the hard to soft reset.

- There is no difference amongst the bias settings or proton energies.

8.2.10.Global Photo Response Non Uniformity

8.2.10.1.During Radiation

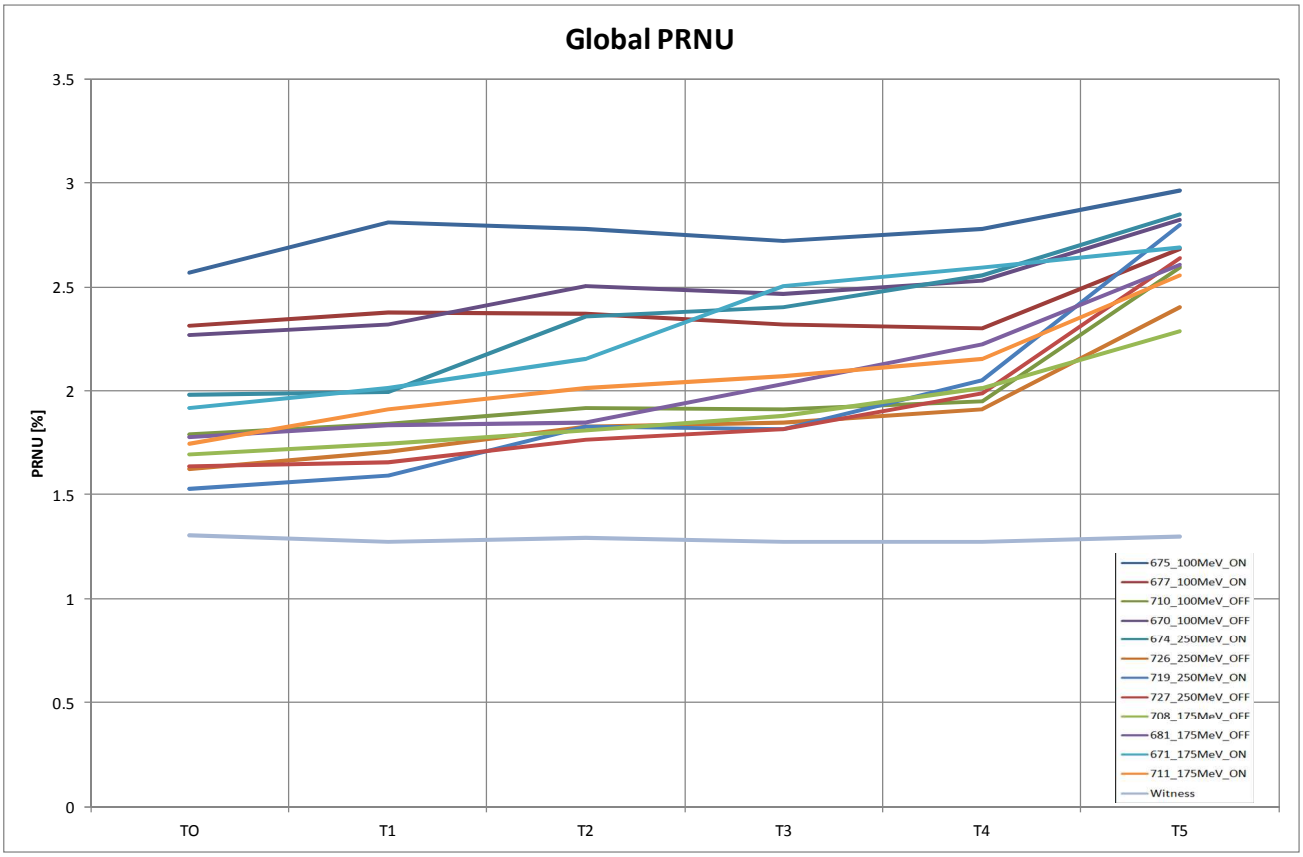

Figure 8-27: Global PRNU vs radiation for different proton energies

The following observations are made:

- According to the above graph, PRNU is increasing with radiation. This is a wrong interpretation as PRNU is increasing due to the sensitivity which is going down with increased radiation. PRNU is expressed as (standard deviation / average grey value). If the average grey value goes down, the PRNU goes up.

- There is no difference amongst the bias settings or proton energies.

8.2.10.2.During Annealing

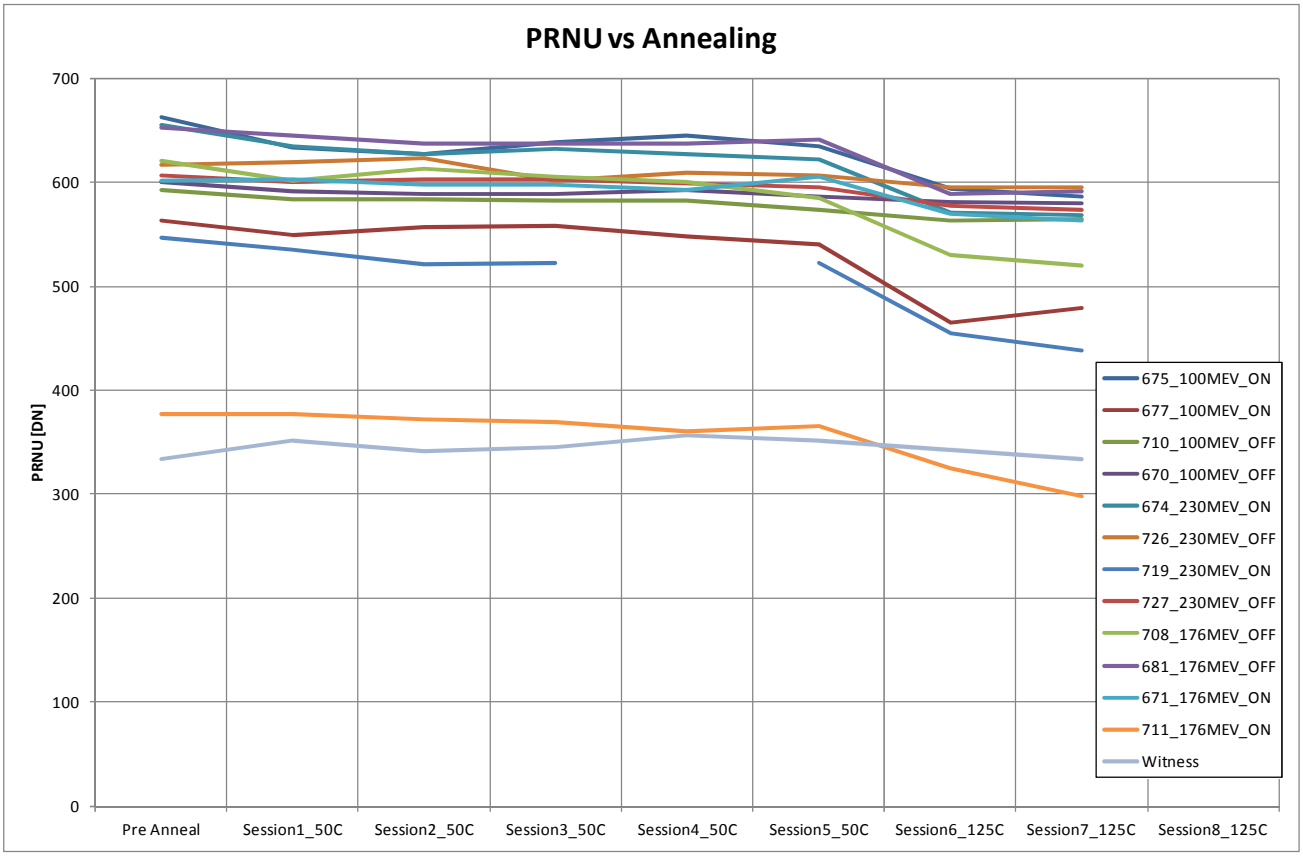

Figure 8-28: Global PRNU vs annealing for different proton energies

The following observations are made:

- PRNU is not changing during the 50C annealing period.
- PRNU is slightly decreasing during the 125C annealing period.

8.2.11. Local Photo Response Non Uniformity

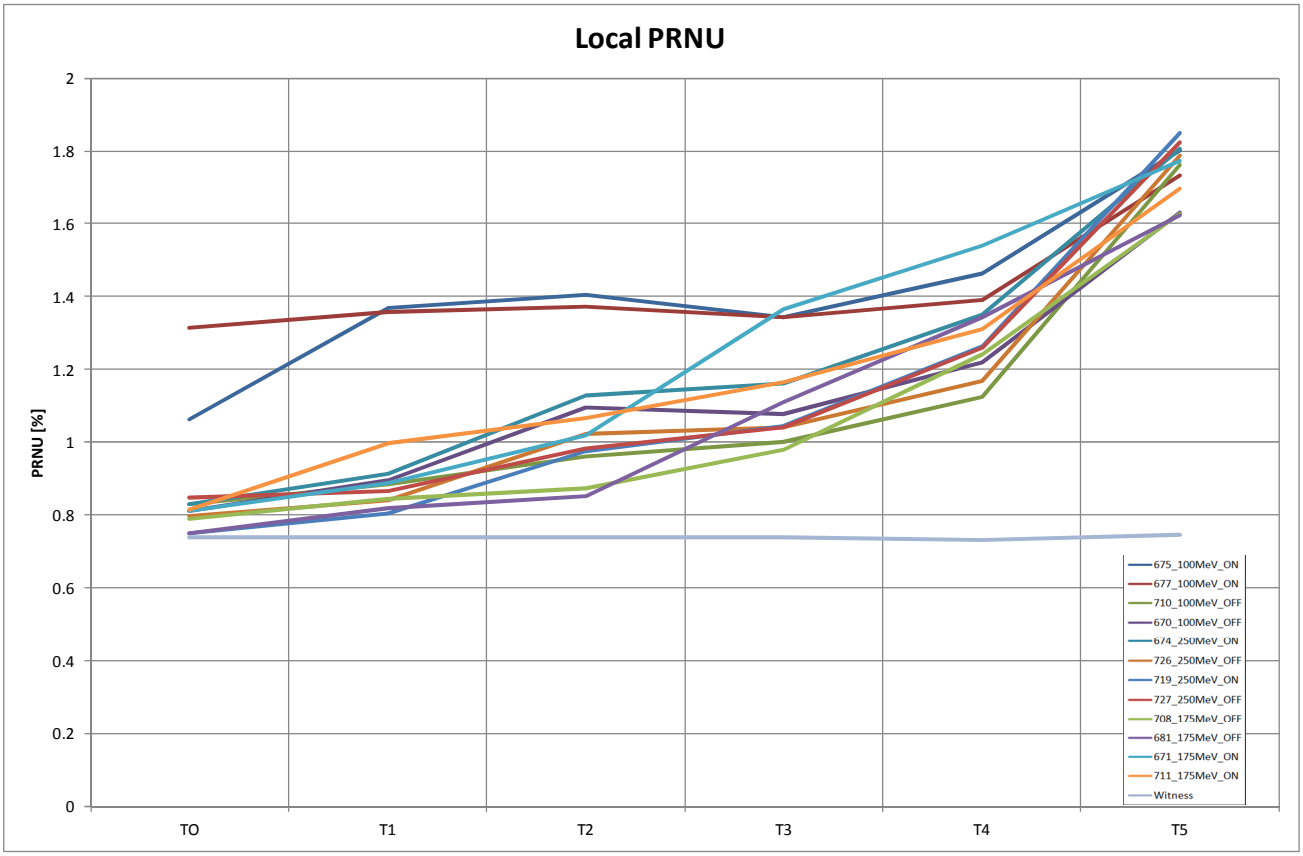

Figure 8-29: Local PRNU vs radiation for different proton energies

The following observations are made:

- According to the above graph, PRNU is increasing with radiation. This is a wrong interpretation as PRNU is increasing due to the sensitivity which is going down with increased radiation. PRNU is expressed as (standard deviation / average grey value). If the average grey value goes down, the PRNU goes up.

- There is no difference amongst the bias settings or proton energies.

8.2.12.Average Grey

8.2.12.1.During Radiation

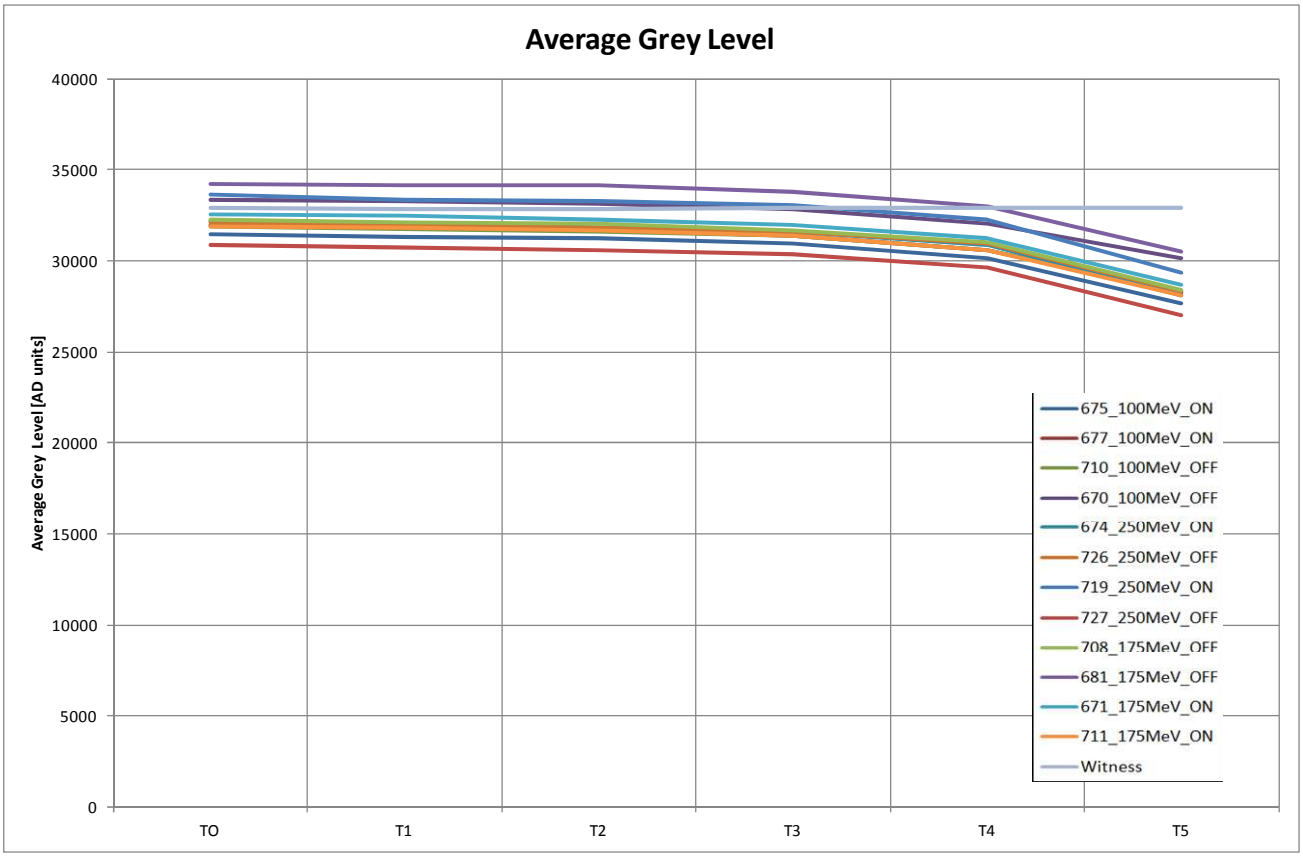

Figure 8-30: Average grey level vs radiation for different proton energies

The following observations are made:

- The average grey level is decreasing during the T4 and T5 radiation session. This is due to the decreased QE.

8.2.12.2.During Annealing

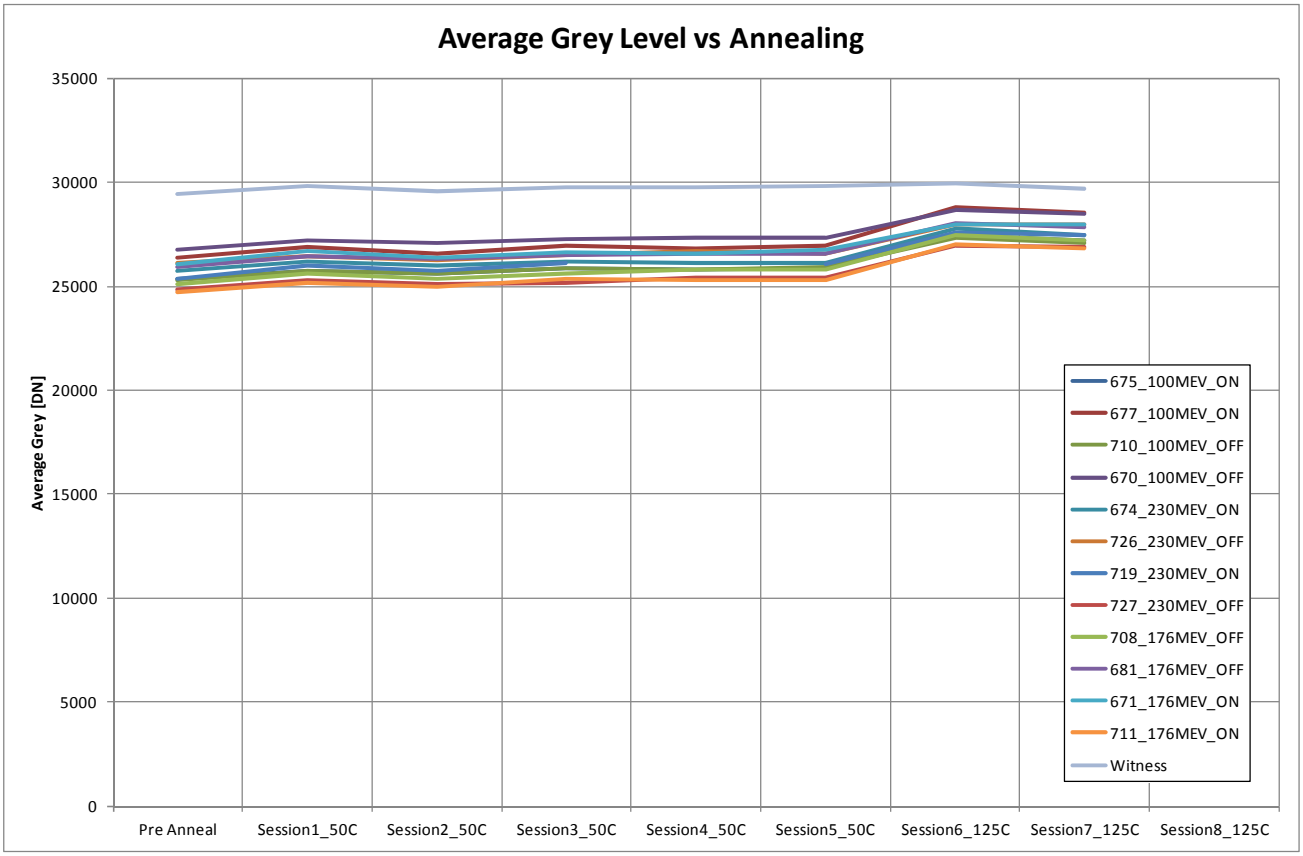

Figure 8-31: Average grey level vs annealing for different proton energies

The following observations are made:

- The average grey level is slightly increasing during the 50C annealing step and is significantly increasing during the first part of the 125C annealing.

8.2.13.Operating Current

8.2.13.1.During Radiation

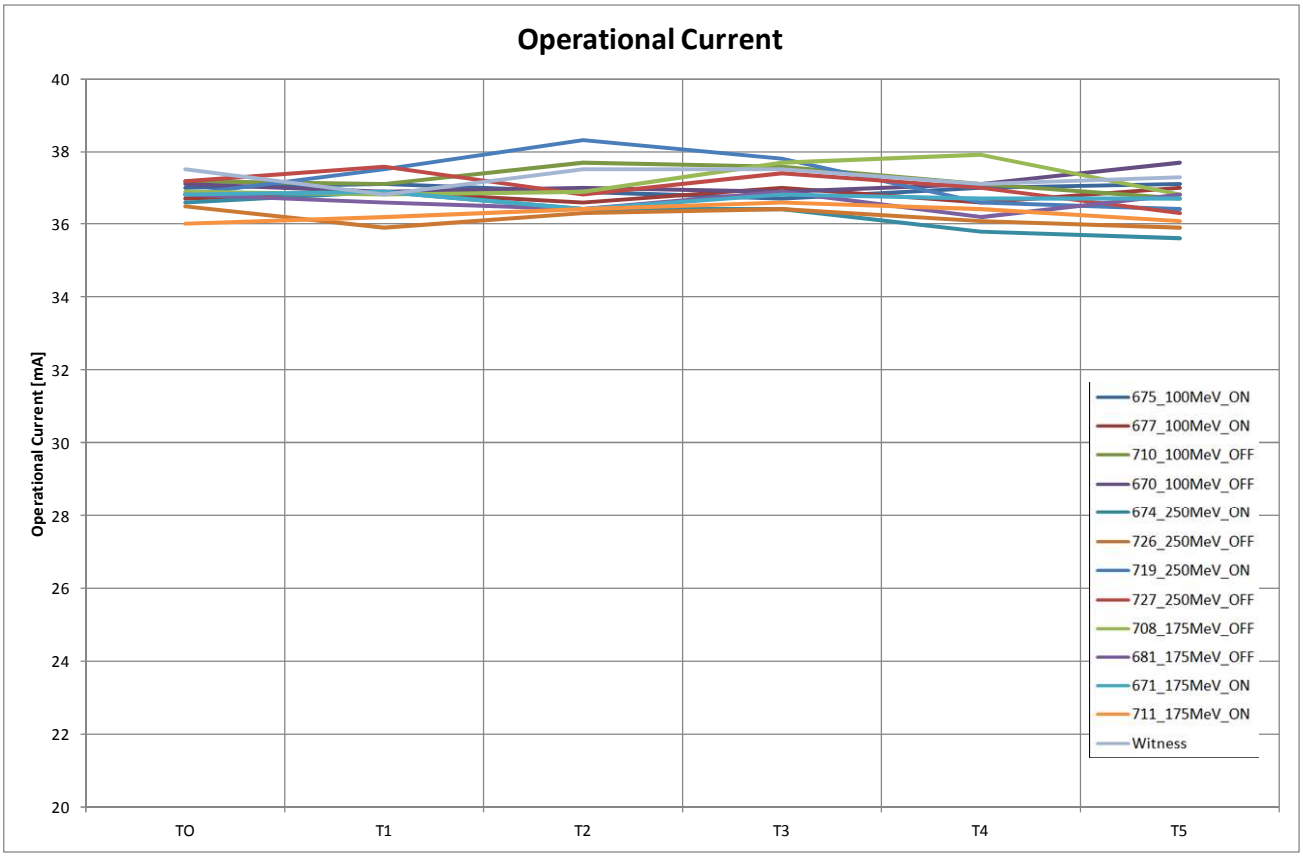

Figure 8-32: Operating Current vs radiation for different proton energies

The following observations are made:

- The operation current does not change over radiation. Also the different biasing schemes and energy levels have no influence.

8.2.13.2.During Annealing

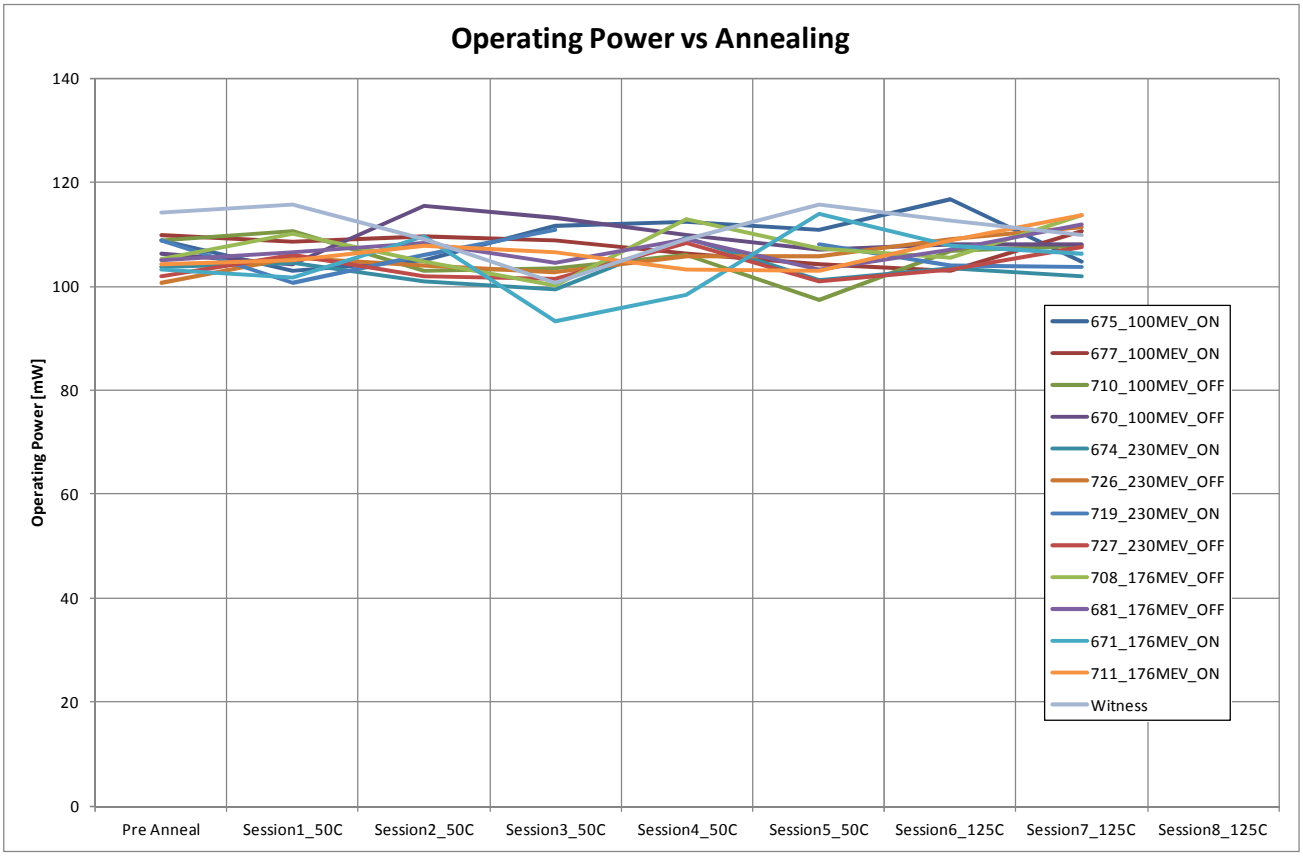

Figure 8-33: Operating Power vs annealing for different proton energies

The following observations are made:

- The operation power does not change over annealing.

8.2.14.Standby Current

8.2.14.1.During Radiation

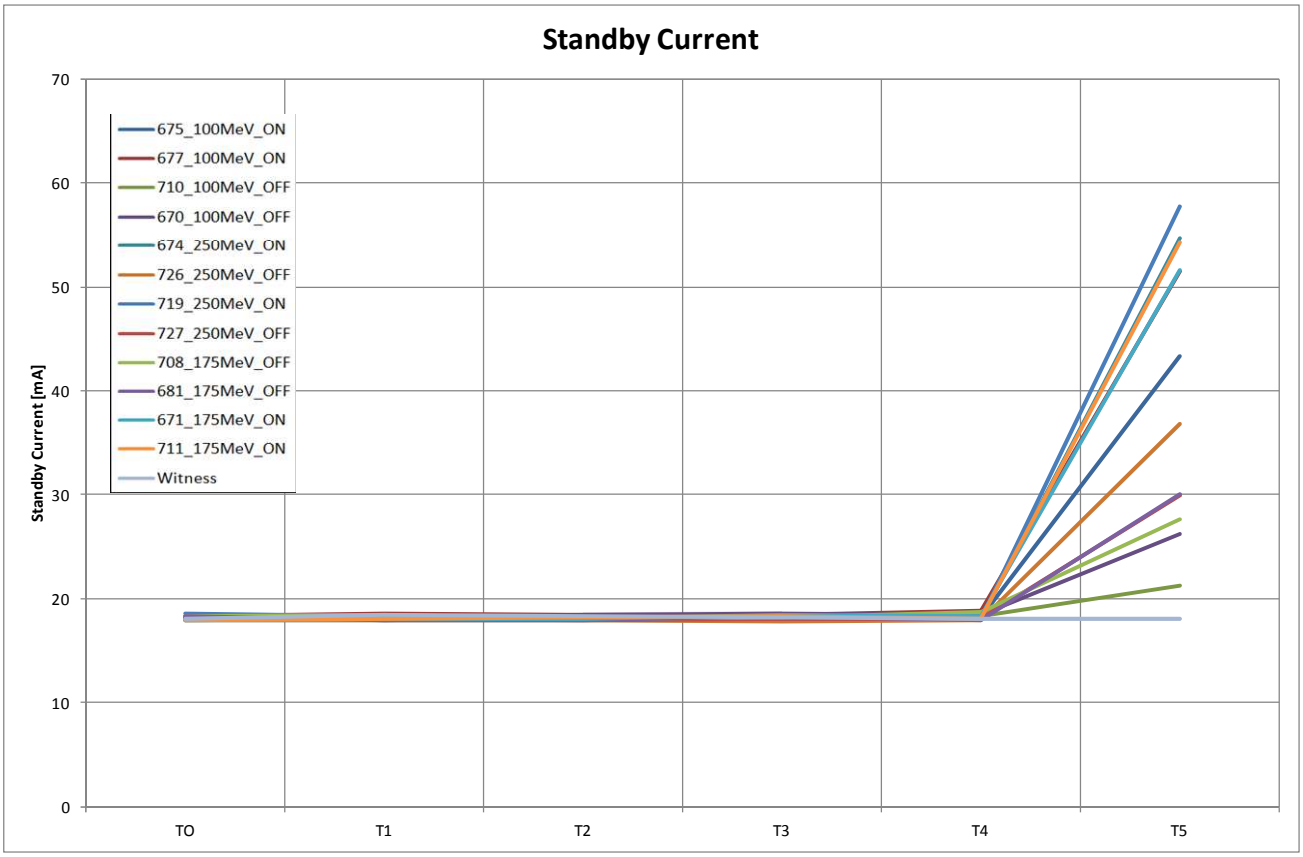

Figure 8-34: Standby Current vs radiation for different proton energies

The following observations are made:

- Standby current is getting unstable after the T5 radiation session. The same observation was made during the evaluation phase in 2007, though the effect was only seen at elevated temperature (85 degC).

- After T5 radiation, the highest standby currents are measured on devices which were in the 'ON' state during radiation; the lowest was measured on the ones which were in the 'OFF' state.

8.2.14.2.During Annealing

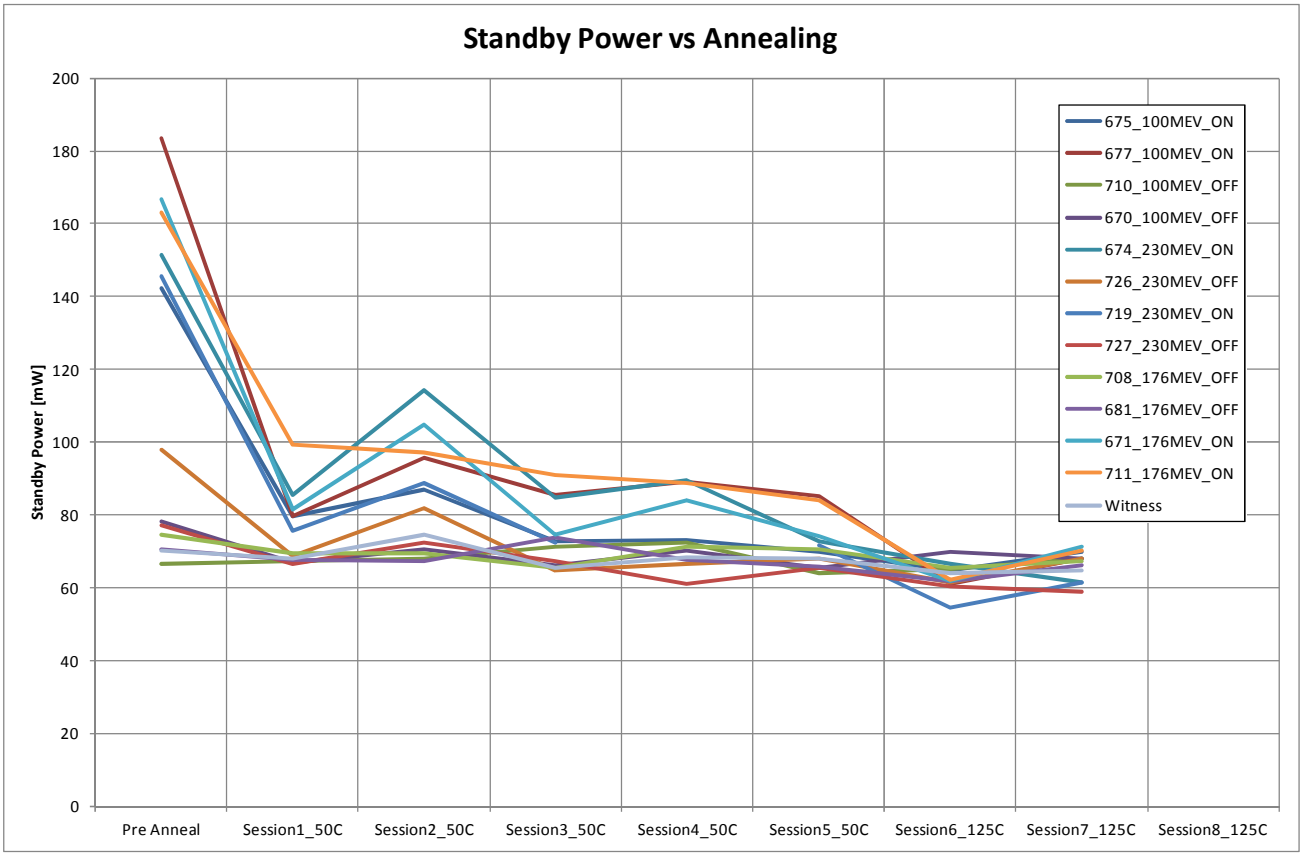

Figure 8-35: Standby Power vs annealing for different proton energies

The following observations are made:

- Standby power is getting less unstable during the 50C annealing period.
- Devices annealed in the ON state showing the highest unstable standby power.
- During the 125C annealing period the standby power is stable again.

8.2.15.DSNU

8.2.15.1.During Radiation

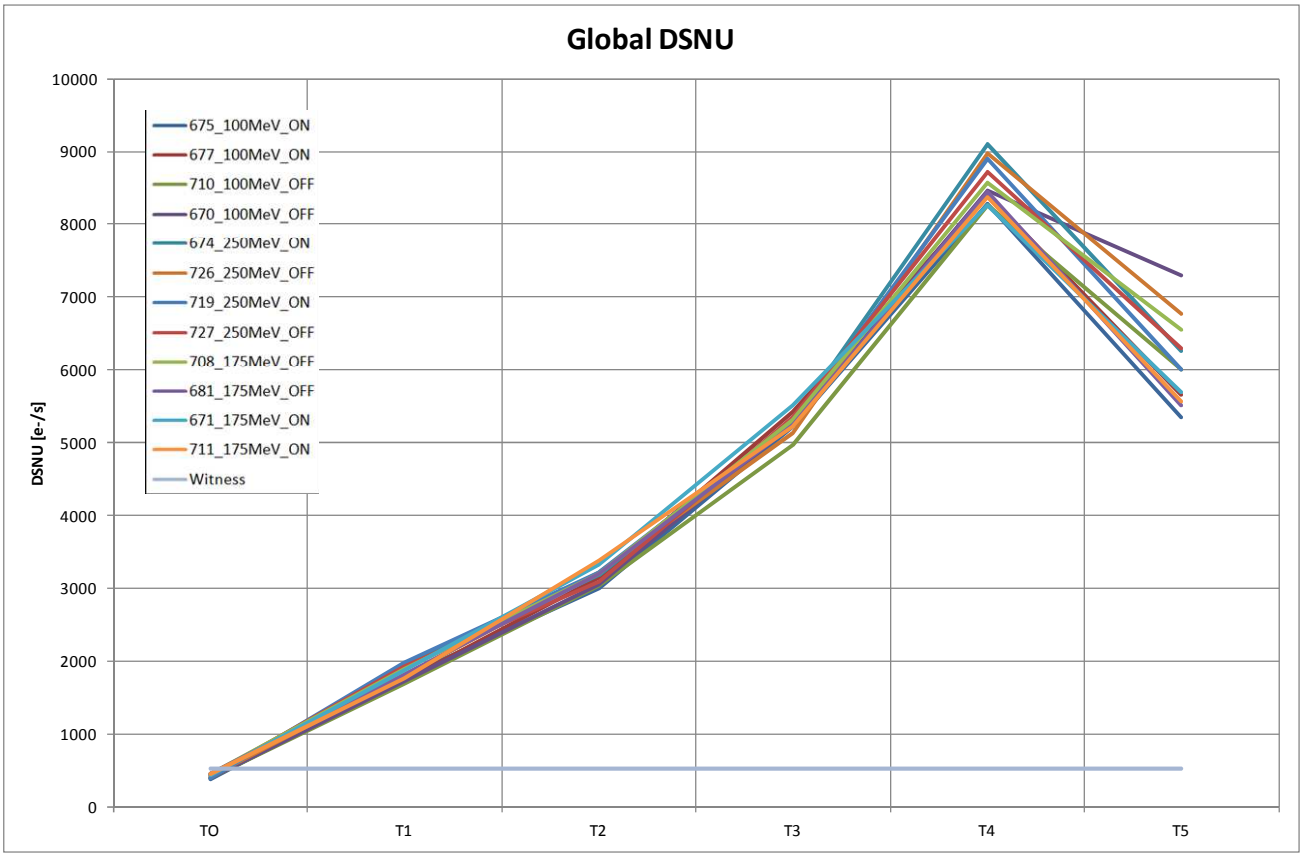

Figure 8-36: DSNU vs radiation for different proton energies

The following observations are made:

- DSNU increases the same for all the samples, independent from the biasing conditions and energy levels.

- After the T5 radiation session, the DSNU is dropping. This is because more and more pixels are saturated and hence decreases again the standard deviation.

8.2.15.2.During Annealing

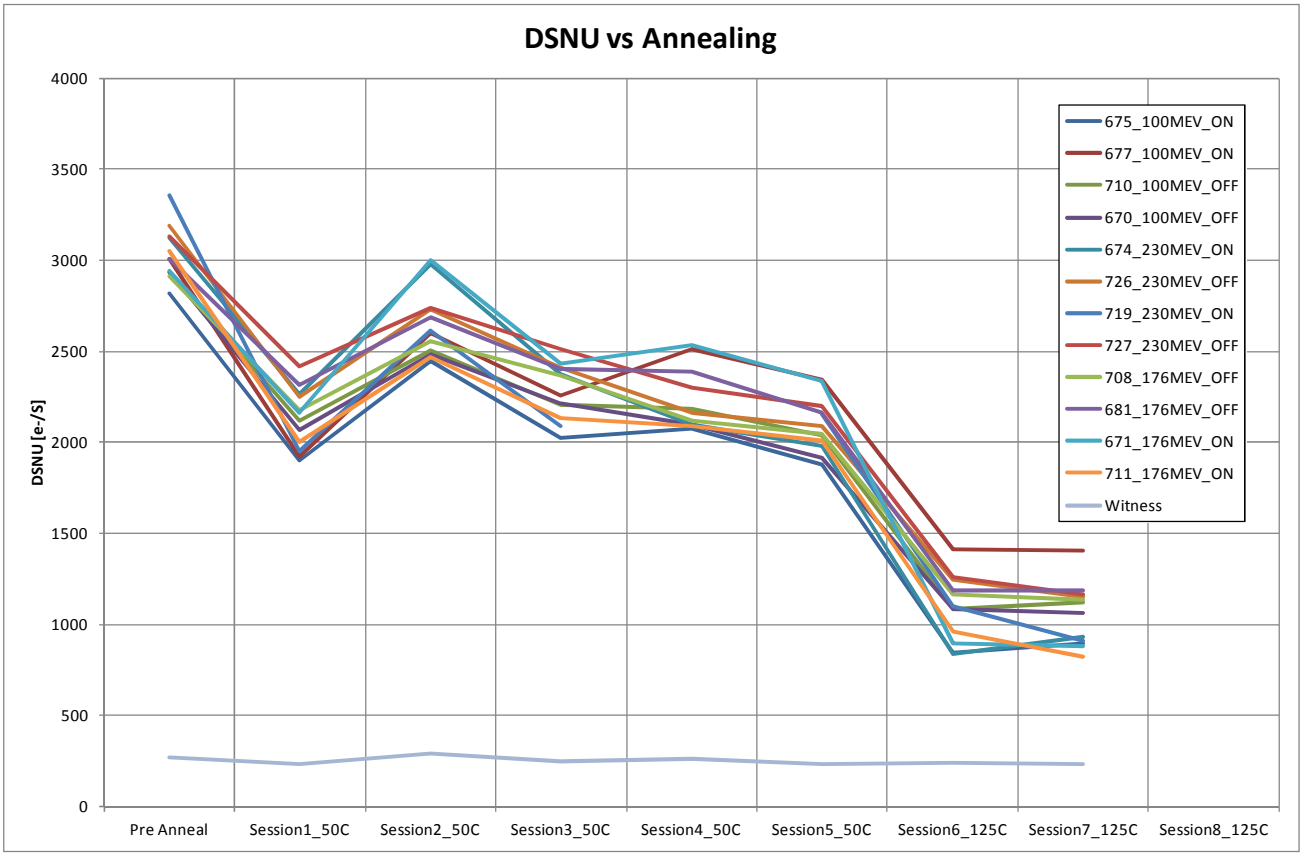

Figure 8-37: DSNU vs annealing for different proton energies

The following observations are made:

- The DSNU is slightly decreasing during the 50C annealing period. The instability is due to the fact that testing is performed at uncontrolled temperature.

- DSNU is further decreasing during the 125C annealing period. The instability is due to the fact that testing is performed at uncontrolled temperature.

- The decrease of DSNU is stopping already after 1 day of 125C annealing.

8.2.16.INL

8.2.16.1.During Radiation

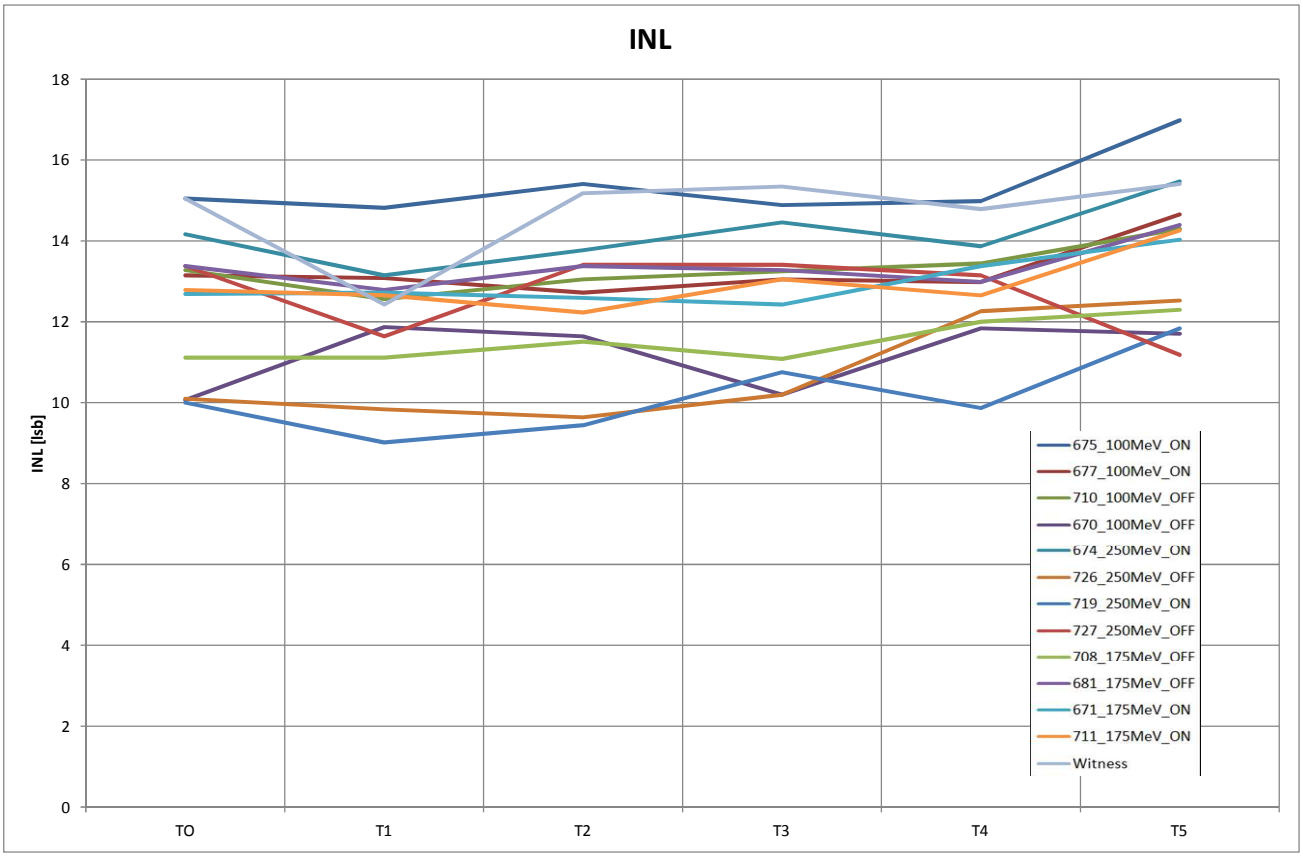

Figure 8-38: INL vs radiation for different proton energies

The following observations are made:

- There's no increase or decrease visible during radiation.

8.2.16.2.During Annealing

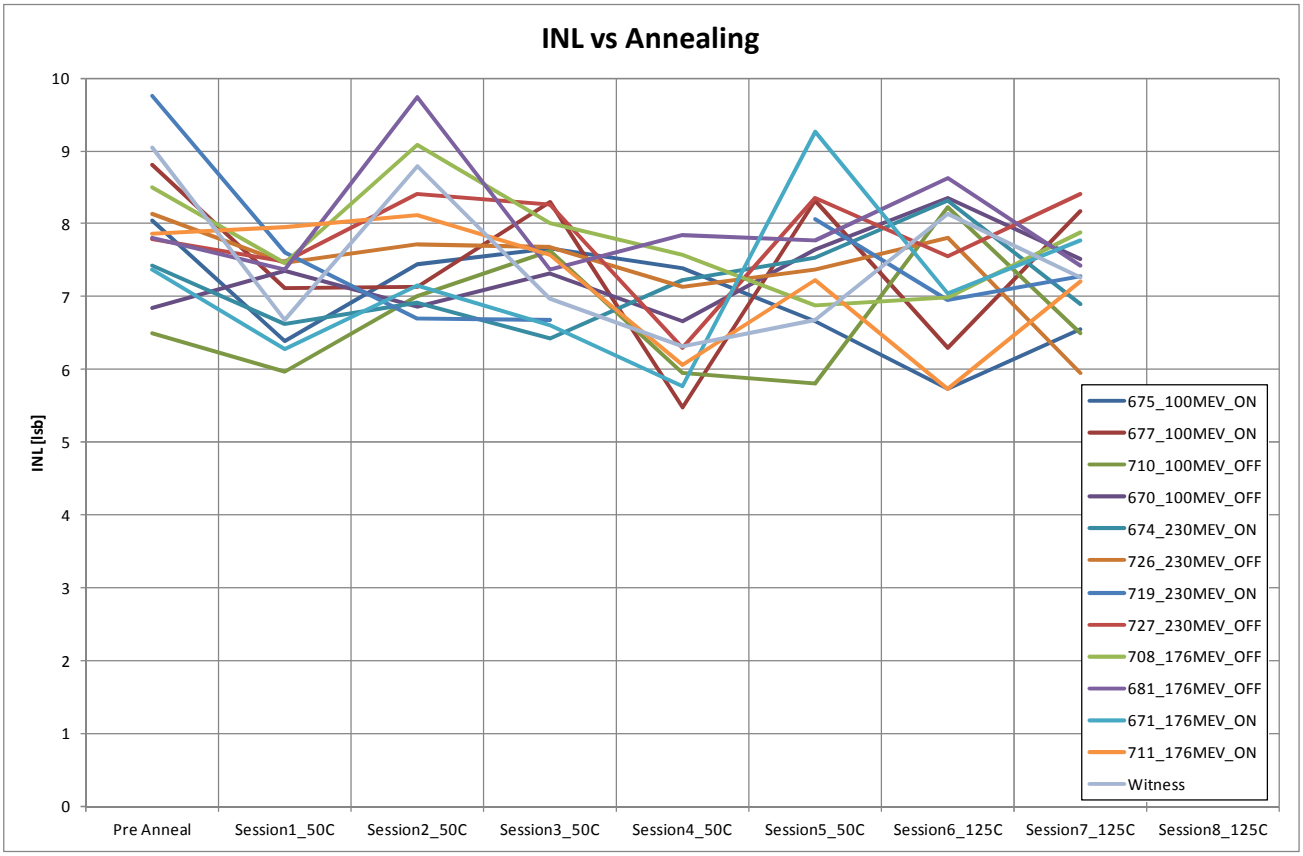

Figure 8-39: INL vs anenaling for different proton energies

The following observations are made:

- There's no increase or decrease visible during annealing.

8.2.17.DNL

8.2.17.1.During Radiation

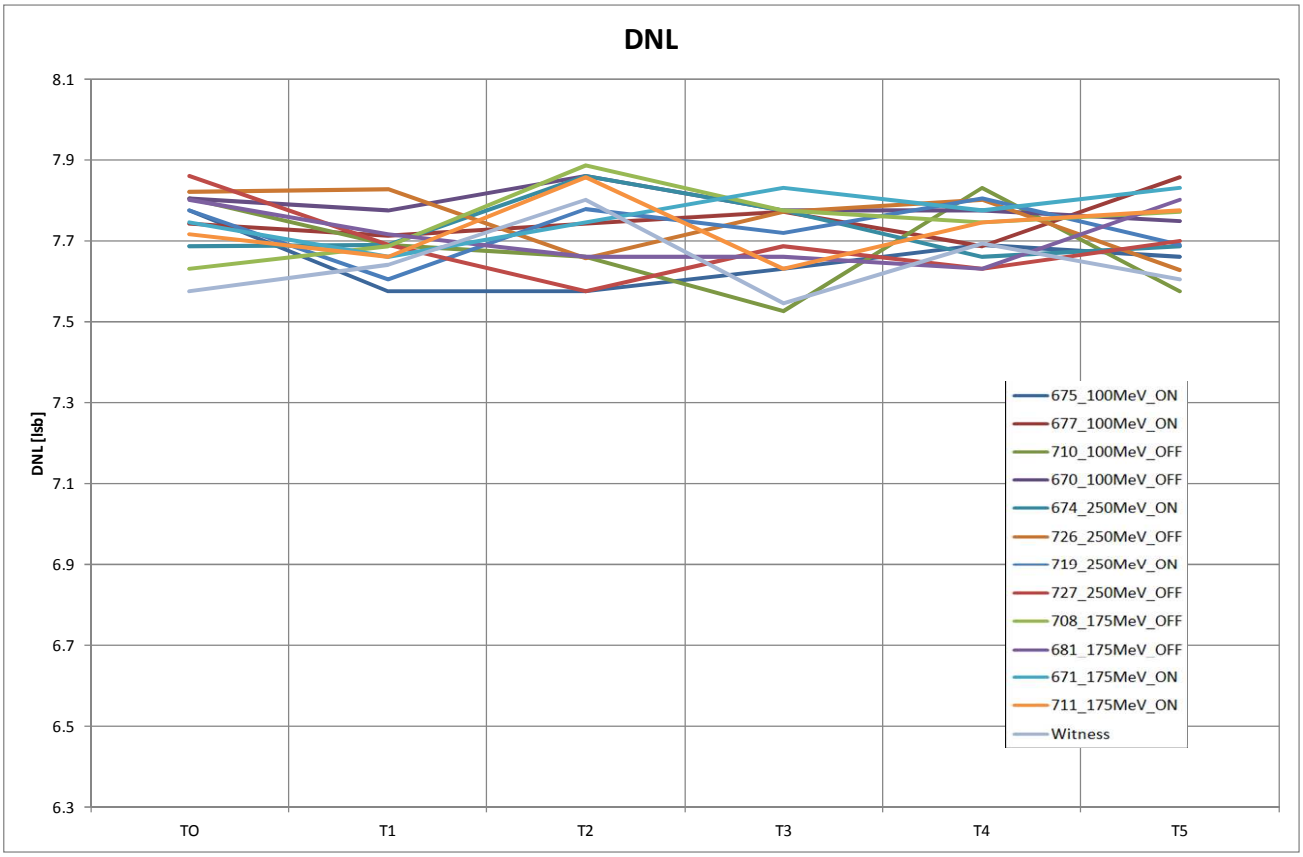

Figure 8-40: DNL vs radiation for different proton energies

The following observations are made:

- There's no increase or decrease visible during radiation.

8.2.17.2.During Annealing

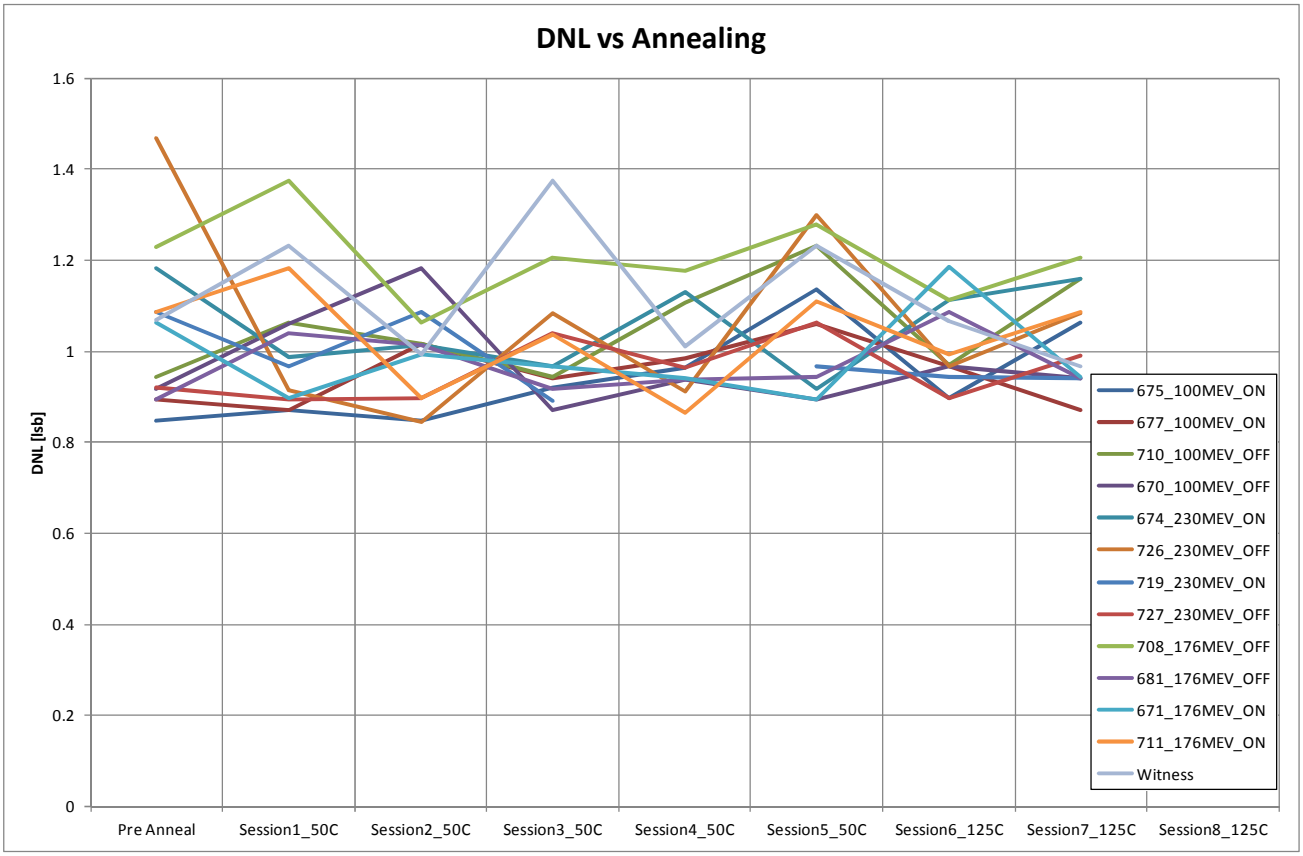

Figure 8-41: DNL vs annealing for different proton energies

The following observations are made:

- There's no increase or decrease visible during annealing.

8.2.18.Electro Optical Measurements

Due to the unforeseen long activation period of the radiated devices, electro optical testing was not performed after the devices returned from the radiation facility.

9.CONCLUSIONS

9 Devices have been subjected to proton energies of 100MeV, 176MeV and 230MeV with several bias conditions.

The following main observations were made on the reported electrical test parameters during radiation and annealing:

- The dark current dispersion of the 9 devices amongst the several radiations is very low. There is also no difference in dark current increase between devices radiated in the ON state and the OFF state.

- Dark current is annealing faster on devices in the ON state.

- The high temperature effect on the dark current and on the DSNU is already effective after 1 day and does change anymore the days after.

- A QE loss is observed after the devices being irradiated with +/- 5.0E+11 particles/cm^2. The QE loss is annealed during the 125C annealing period.

- The standby current gets unstable after +/- 1E+12 particles/cm^2. During the 50C annealing the currents are less unstable to be totally stable after the 125C annealing.

- FPN in HTS reset mode is increasing significantly during the first 3 irradiation sessions, to come back to its initial value during T4 and T5 irradiation sessions. This phenomenon was also observed during the neutron testing (other location, other date). The reason for this behavior is unknown but is most likely related to the driving electronics of the hard to soft reset.

The annealing period could only take place 7-8 months after the irradiations took place due to the activation of the parts. The radiation facility was not allowed to ship the parts until the activation energy was under a certain level.

Due to the above electro-optical testing after radiation and annealing has been skipped.